Research Square

Preprints are preliminary reports that have not undergone peer review.
They should not be considered conclusive, used to inform clinical practice,
or referenced by the media as validated information.

Landslide Triggered by Orthogonal Tunnel Excavation and Prevention Measures in Jimei Village, Sichuan Province, China

zhongfu wang (xfjtwzf@163.com)
North China University of Water Resources and Electric Power https://orcid.org/0000-0003-1800-5435
Han Dong Liu
North China University of Water Resources and Electric Power
Si Ming He
Institute of Mountain Hazards and Environment Chinese Academy of Sciences
Yunfeng Fang
Hydrochina Huadong: Hydrochina Huadong Engineering Corp

Research Article

Keywords: tunnel-landslide system, ancient landslide, stability evaluation, deformation monitoring, numerical simulation, prevention measures

Posted Date: May 27th, 2021

DOI: https://doi.org/10.21203/rs.3.rs-530013/v1

License: This work is licensed under a Creative Commons Attribution 4.0 International License.
Read Full License

Landslide triggered by orthogonal tunnel excavation and prevention measures in Jimei Village, Sichuan Province, China

Zhong Fu Wang[1,2,3] (Corresponding author) **E-mail:xfjtwzf@163.com**

Han Dong Liu[1,2] **E-mail:Liuhandong@ncwu.edu.cn**

Si Ming He[4] **E-mail:hsm@imde.ac.cn**

Yunfeng Fang[5] **E-mail: fang_yf@ecidi.com**

1.North China University of Water Resources and Electric Power. Zhengzhou 450046, China

2. Henan Key Laboratory of Geotechnical and Structure Engineering. Zhengzhou 450046, China

3. Research Center on Levee Safety and Disaster Prevention, MWR, Zhengzhou 450003, China

4. Institute of Mountain Hazards and Environment, Chinese Academy of Sciences, Chengdu 610041, China.

5. Zhejiang Huadong Construction Engineering Co., Ltd, Hangzhou 310014, china

Abstract: The axis of highway tunnels constructed in mountains under complex geological conditions is usually orthogonal to the section of potential landslide. The tunnel construction may lead to landslide, which then may result in the deformation and/or cracking of tunnels. Therefore, it is very important and practical for tunnel projects to study the complex interaction mechanism between orthogonal tunnel and landslide and provide appropriate prevention measures for tunnel. This paper, on the base of geological survey, on-site monitoring and numerical simulation, analyzed the deformation and reason of an ancient landslide revived by tunnel construction and studied the prevention measures for tunnel. The results show that the reason for the revival of the

ancient landslide resulted mainly from the tunnel construction through sliding surface, and the ancient landslide is generally stable because most landslide deformation occurred beyond the tunnel and in the upper part of landslide. The numerical simulation was used to optimize the tunnel prevention scheme by the analysis to the stability, stresses and deformation of landslide based on stress-strain control theory. The original anti-slide pile design was cancelled and finally the tunnel is reinforced by upper soil removal and moving upper soil into toe. This tunnel has successfully completed and are under good operation. The used prevention measures were proven to be effective according to the monitoring data about displacements and stress of landslide and tunnel during operation period, and saved about seven million US$. The research results in this paper may offer a beneficial reference to projects with similar geological conditions.

Keywords: tunnel-landslide system, ancient landslide, stability evaluation, deformation monitoring, numerical simulation, prevention measures

1. Introduction

China suffers from abundant severe geological hazards each year, and more than 65% of these hazards are statistically landslides (Technical Guidance Centre for Geological Disasters, 2019). When various tunnels are constructed in the mountains in southwestern China, it is very difficult to avoid potential large landslides due to the insufficient instigation on complex geological conditions, although the distance between tunnels and potential landslides are set to be as far as possible in the initial design stage. Tunnels may interact strongly with landslides during tunnel construction and operation. Slopes may creep or even slide due to tunnel construction, and then tunnels suffer from deformation and cracking due to slope failure, which could pose a great threat to the construction safety and operation of tunnel (Karakus and Fowell, 2005; Tang et al., 2014;

45 Bandini et al., 2015; Bayer et al., 2017; Komu et al., 2019; Vassallo et al., 2019).

46 At present, some scholars have paid more attention to the interaction between tunnels and
47 landslides and the damage to engineering structures, and have obtained some achievements.

48 Ruggeri et al. (2016) analyzed the deep-seated landslide which was triggered during the
49 excavation of the Piscopio I tunnel of the new Ionian national road in Italy, and then provided the
50 suitable stabilizing measures. Zhang et al. (2017) analyzed the interaction between tunnel and
51 landslide in mountain area, and studied the minimum safety distance between tunnel vault and
52 sliding belt and its influence factors on the base of the slip-line theory. Zhou et al. (2020) analyzed
53 the structural damage of tunnel concrete and sidewalls induced by loess landslide and investigated
54 the landslide deformation. The interaction between a slow-moving landslide in clay soil and a
55 railway tunnel protected by sheet pile walls, which goes through the landslide accumulation, was
56 presented by long-term deformation and stress monitoring and FEM modelling (Vassallo et al.
57 2016, Mishra et al. 2017, Minardo et al. 2018, Vassallo et al., 2019).

58 Konagai et al. (2005) analyzed the landslide-induced damage to Kizawa tunnel in the 2004
59 Mid-Niigata Prefecture earthquake in Japan. Kaya et al. (2015) conducted a comprehensive
60 analysis to the slope failure mechanism triggered by the excavation of Arakli tunnel by kinetics,
61 limit equilibrium method and numerical simulation. Jiao et al. (2013) assessed the effect of two
62 coal mine tunnels on an ancient landslide by using borehole data, deformation monitoring and
63 numerical simulation, and the results show that the landslide is generally stable, partially with
64 shallow slope failure. De-pei et al. (2002) and Jian-qiang et al. (2002) studied the relationship
65 between tunnel deformation and landslide, presented five geological models for their relationship,
66 and proposed an idea that landslide may be predicted by tunnel deformation. Tao and Zhou (2003,

67 2007) analyzed the landslide-tunnel interaction and deformation based on three types of geological
68 mechanical models, and concluded that the distance between tunnel and sliding surface is the key
69 factor for tunnel deformation. Liu et al. (2012) carried out a preliminary analysis to various
70 geological problems and treatment measures for Chuanzhusi highway tunnel through ancient
71 landslide. Ma (2003, 2007) established the tunnel-landslide interaction theory on the base of
72 tunnel type and geological model, and analyzed the tunnel and landslide deformation mechanism
73 and stabilizing measures under consideration of parallel, oblique and orthogonal directions.

74 The above research results show that tunnel-landslide systems differ greatly in stress and
75 deformation. Generally, the tunnel-landslide interaction decreases with increasing distance.
76 Moreover, when the tunnel orthogonally crosses the landslide, especially crosses the sliding belt of
77 thick landslide, they will interact heavily with each other, which finally results in the strong
78 cracking and deformation of tunnel and then poses a great threat to projects. This paper took the
79 example of Jimei tunnel in southwest China orthogonally across a 60m thick ancient landslide,
80 and analyzed the tunnel-landslide deformation and prevention measures based on geological
81 survey, on-site monitoring and numerical simulation.

82 2. Regional geological setting

83 As a part of S26 highway in Sichuan Province in China, the Xuyong-Gulin highway begins
84 from Xuyong County, Luzhou City, and ends at Erlang Town, Gulin County, as shown in Fig. 1.
85 The study area is north of Yunnan-Guizhou Plateau and south of Sichuan Basin, generally with
86 low terrain in the northwest and high terrain in the southeast. The study area belongs to
87 medium-mountain landform, and steep scars here are well developed, with highest elevation of
88 1843m, lowest elevation of 700m, and height difference of more than 1000m.

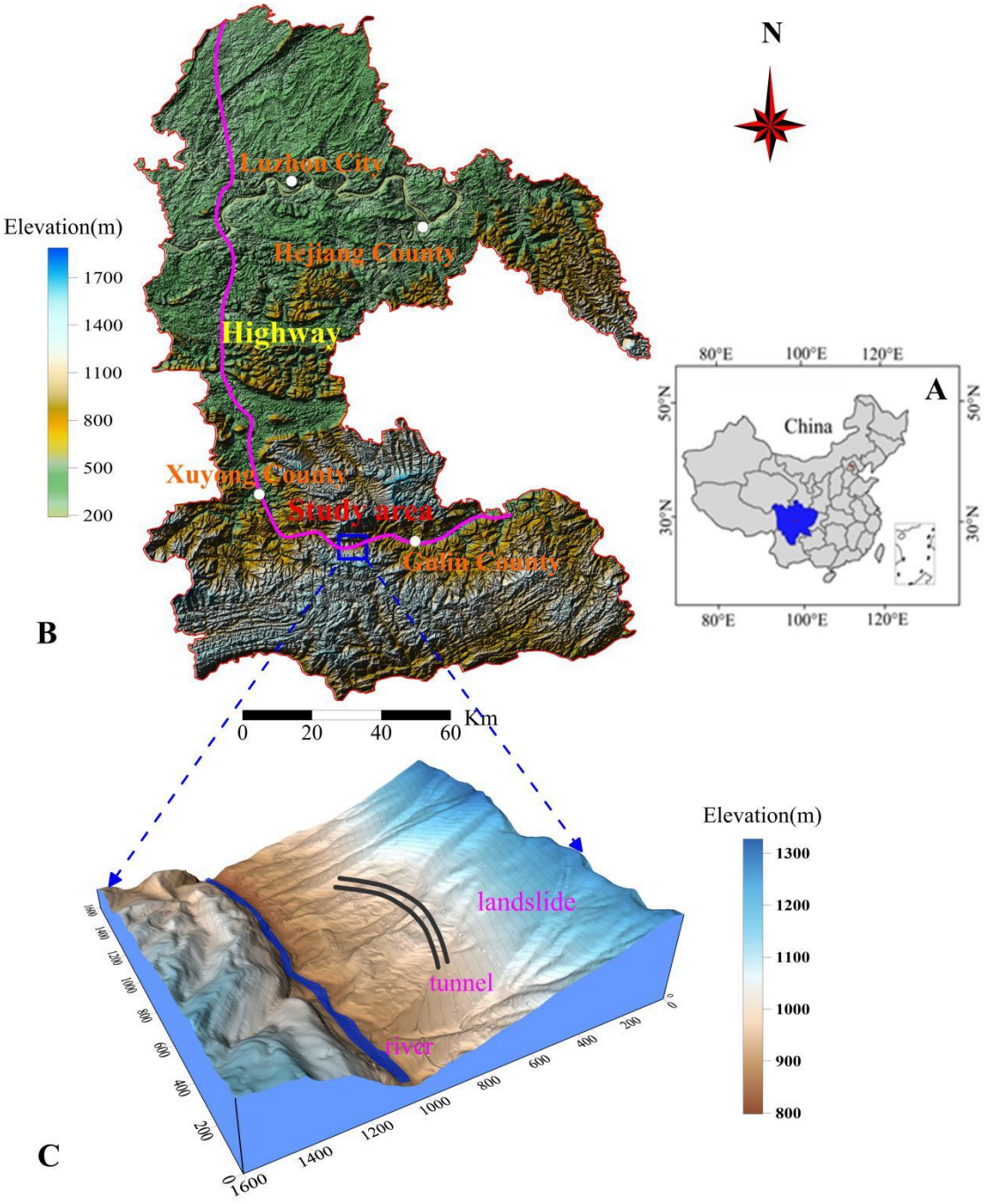

Fig.1 Location of Jimei tunnel. (A) schematic location in china; (B) location of Xuyong-Gulin highway; (C) 3D terrain of Jimi tunnel and landslide.

The geological survey results indicate that the strata in the study area, from top to bottom, consist basically of: (1) artificial Miscellaneous fill (Q_4^{me}), generally distributed in the subgrade range; (2) landslide accumulation layer (Q_4^{del}), found in the landslide range; (3) colluvium and

95 diluvium layer (Q_4^{c+dl}), with gravel, block stones and gravel silty clay, which is basically in the
96 slope at the landslide tail; (4) alluvial and pluvial layer (Q_4^{al+pl}) of sub-circular and sub-angular
97 boulders, basically distributed in the stream riverbed (Fig. 1); (5) upper Member of middle
98 Jurassic Shaximiao Formation (J_2s^2), consists mainly of interbedded fine mudstone and silty
99 sandstone of various thicknesses; (6) lower Member of middle Jurassic Shaximiao Formation
100 (J_2s^1), made mainly of argillaceous siltstone and siltstone, partially with fine sandstone lens and
101 oil shale.

102 The about 23km long Baiyangping syncline, with approximate West-East (WE) axis and
103 eastward inclination, has a great effect on the study area because the study area is located in the
104 southeast part of the syncline. The study area is a bedding slope with predominant attitude of 13°
105 ∠37º - 55°∠15°, obviously steep at slope back and gentle at slope front. In the fine sandstone,
106 there are two developed sets of joint, namely, L1: 160°-190°∠65°-70º and L2: 250°∠80°.

107 The study area has four distinct seasons, abundant sunshine, and a little rainfall, with most
108 rainfall in the period from May to August and annual precipitation of about 494.4mm.

109 3. Tunnel description and site conditions

110 The Jimei tunnel and landslide are located in the K12+506 - K13+535 section in Jimei
111 Village, Deyao Town, Gulin County, Sichuan Province, China, and the tunnel consists of one
112 978m long left tunnel and 1029m long right tunnel. The landslide approximately has a north dip
113 direction, and the tunnel axis is orthogonal to the landslide profile. During the preliminary design
114 stage, the landslide was identified as an ancient landslide, and then the tunnel was design to be
115 located in the bedrock beyond the landslide. Unfortunately, the tunnel was found to be still
116 through the ancient landslide during the tunnel excavation period. The left tunnel crossed

117 orthogonally the ancient landslide in the ZK12+750 - ZK12+835 region and ZK13+042 -
118 ZK13+107 region, respectively, which resulted in the deformation and cracking of landslide and
119 tunnel.

120 **3.1 Characteristics of ancient landslide**

121 The landslide boundary was determined by the landslide deformation and adjacent terrain
122 (Gu et al., 2017; Pánek et al., 2008). The ancient landslide is generally like W in shape, with slope
123 of about 21°. A nameless stream, which is the branch of Gulin River, flows along the slope toe.
124 The landslide is generally about 700m long and 400-900m wide, steep and wide in the upper part
125 and gentle and narrow in the lower part, with developed gentle platform in the middle and lower
126 part. The slope surface is mostly occupied by farmland, with a preliminary school and many
127 resident houses. The landslide deformation had a direct effect on the tunnel structure and buildings
128 on the slope surface. The ancient landslide was basically stable before tunnel excavation.

129 According to the geological survey and borehole data, the ancient landslide has different
130 characteristics in different zones. The landslide can be divided into two zones (zone I and zone
131 Ⅱ). Zone I, about 980m long and 330m wide, is located in ZK 12+506 – ZK 12+840 section, with
132 main sliding direction of about 354° and average slope of 18.5°, accounting for 53% of the whole
133 landslide area (Fig. 2). Zone Ⅱ, about 550m long and averagely 405m wide, is located in
134 ZK12+840 - ZK13+160 section, with main sliding direction of about 358° and average slope of
135 17.8°, accounting for 47% of the whole landslide area. The borehole data show that the ancient
136 landslide is up to 72.6m thick, averagely more than 50m thick, and the whole landslide is over 11
137 million m^3 in volume, being the giant traction-type deep-seated rocky bedding landslide. This
138 ancient landslide originally slid along weak structural plane, and subsequently suffered from

multi-zone multi-period and multi-layer slides due to long-term exterior forces.

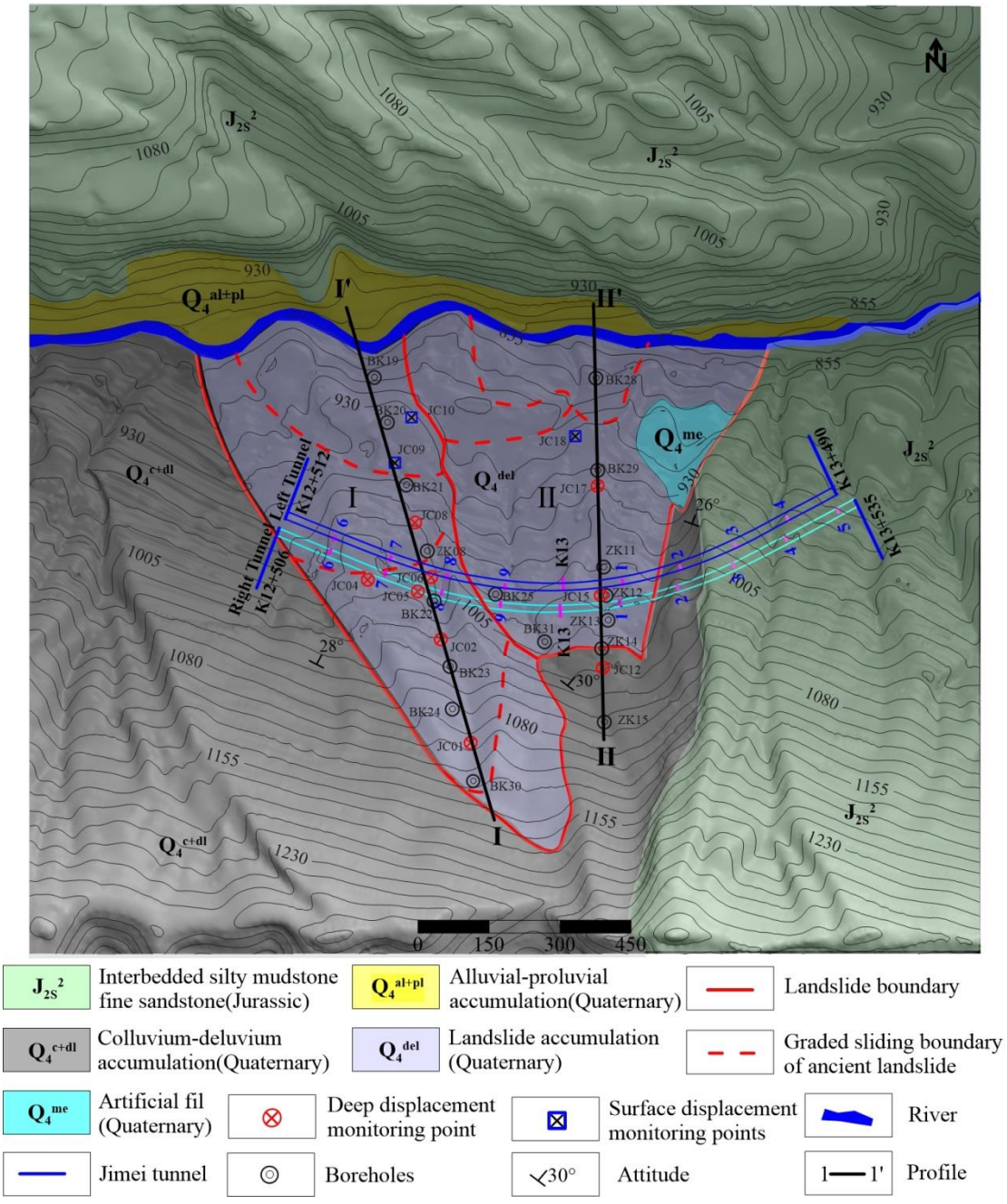

Fig.2 The geological structure of the study area

3.2 Composition of landslide

The sliding body in zone I consists mainly of block stone and gravel, with a little silty clay, and has uneven texture. There are a large number of undisintegrated rocks in zone I due to the incomplete disintegration after slope failure (Fig. 3 and Fig. 4). However, zone II is greatly

146 different from zone I in material components, which consists basically of gravel with breccia clay,

147 plastic to soft plastic, with multi-layer smooth surfaces, partially with 16.5-50.0m long bock stone.

148 The potential failure surface is basically identical to the original failure surface, and some

149 potential sliding surface is directly on the underlying bedrock.

150

151 **Fig.3** Core from (A) borehole BK23; (B) borehole BK14.

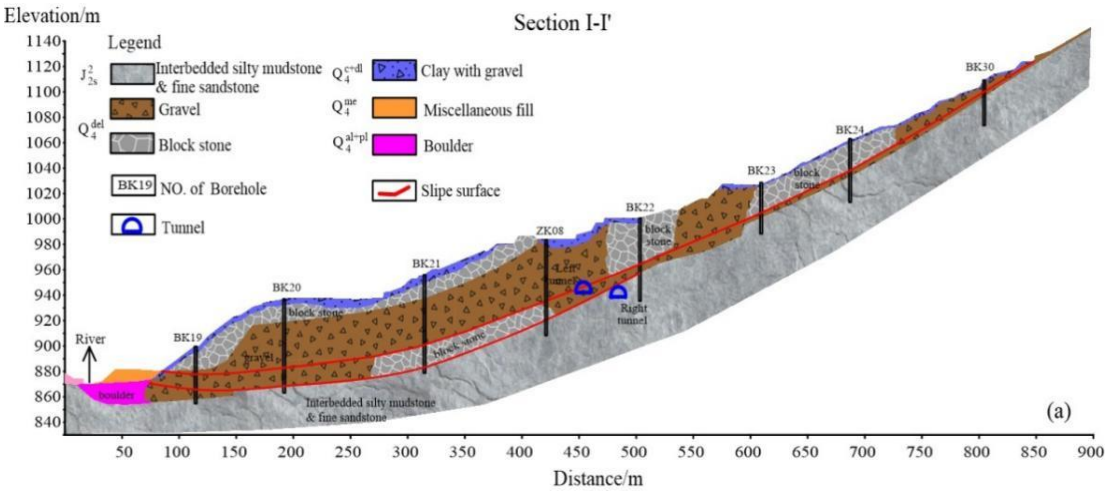

152

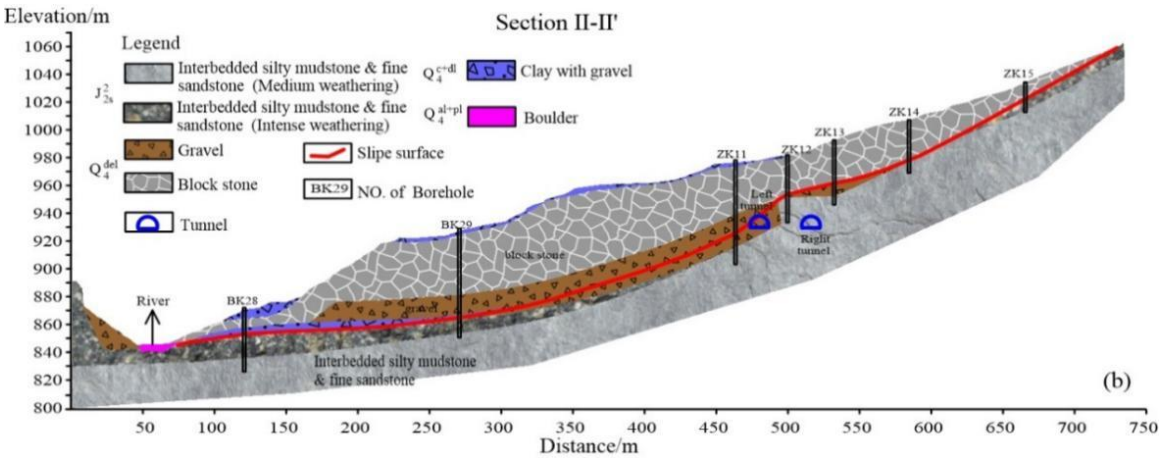

153

154 **Fig.4 Geological profile of (a) 1-1'; (b) 2-2'.**

155 **3.3 Features of sliding surface and sliding bed**

156 According to drilling (Fig.3 and Fig.4), supplementary investigation data by on-site survey
157 (Fig.5), and deformation monitoring (Fig.6), geometry and position of the sliding surface was
158 determined. Both the sliding surface and sliding bed in zone I and zone II share some similar
159 features: (1) sliding happened along weak structural planes, and falls into the category of
160 traction-type bedrock bedding landslide; (2) the sliding surfaces were greater than 60m in the front
161 and middle sections, with large scale; (3) have experienced multi-zone, multi-stage, and
162 multi-layer slide.

163 However, there are many differences between the two zones: (1) in longitudinal direction, the
164 sliding surface of zone I is gentle and smooth, with gentle undulation, and the middle and back
165 sections are steep; while that of zone II is greatly undulating, and the middle and back sections are
166 gentle. In transverse direction, zone I varies sharply in the sliding surface boundary, with bedrock
167 scarp found at the eastern boundary; while zone II changes greatly in thickness, largely undulating.
168 (2) All the sliding surfaces were found in the regions with adverse engineering geology, but for
169 zone II, the sliding surface is mainly along the weak oil shale which is the interface between J_{2s}^{2}

and J_{2s}^{1}; for zone I, the sliding surface is generally along the weak structural plane in J_{2s}^{2}. (3) The bottom of sliding body in zone II is 5-25m lower than that in zone I, with more energy release, and is above the adjacent riverbed. However, sliding surface of in zone I is below the riverbed, and thus riverbed provides some resistance to this sliding body. Thus, the bottom of sliding body in zone I has better stability.

3.4 Formation mechanism of ancient landslide

The ancient landslide was originally developed in a bedding bedrock form, which was affected by many factors such as strata attitude, structure, groundwater, river corrosion, and slope angle.

The landslide is located at a bedding slope in the southwest of Baiyangping syncline. The slope has an attitude of 32°∠15° - 26° with steep upper part and gentle lower part (Fig. 2), and the slope consists of sandstone-mudstone interlayer of Jurassic Shaximiao Formation. There is abundant fractures in the sandstone, which could help groundwater flow rapidly. In addition, there are two sets of joints in the slope, approximately normal to each other, which tends to be subject to tension and lateral shearing. The infiltration of surface water through fractures can lead to large pore water pressure, retains on the impervious mudstone surface, and thus poses a great threat to slope stability by softening the mudstone and reducing its mechanical parameters. Furthermore, the long-term river corrosion against slope toe resulted in the high and steep scar, and finally large-scale bedding landslide happened due to rainfall, forming the initial ancient landslide. Subsequently, many years of weathering, rainfall, corrosion and human activities shaped the current landslide. No deformation happened in the ancient slope since the last 100 years, and the slope was generally stable before the tunnel excavation.

4. Deformation characteristics of landslide and tunnel

The slid bedrock has not yet fully disintegrated, and thus it is difficult to distinct the true bedrock from false bedrock. Therefore, the tunnel did not completely avoid the ancient landslide, and goes through zone I and zone II. In August 2014, the left tunnel was firstly excavated in sliding body of zone II from the chainage ZK13+107, and finally went through the sliding body of 103m length successfully by means of strong reinforcement and the adjustment of construction method in January 2015, without deformation and cracks later. The tunnel entered subsequently into zone I, with the whole ZK12+835 to +516 section of left tunnel in sliding body, and the sliding surface crossed obliquely the top left of right tunnel in K12+720 to +506 section. As a result, over 300m long tunnel passes through the ancient landslide. The excavation of right tunnel in zone I resulted in the cracks on ground surface, cracks & deformation on tunnel, and deformation in soil.

4.1 Landslide deformation and emergency monitoring

Some arc-shaped cracks with 10-40cm width and 5-20cm depth occurred in the region about 270m right from tunnel, over 500m long intermittently, and generally transfixed at the landslide tail. Much evidence indicated that partial ancient landslide on the right side of the tunnel in zone I was reactivated by the tunnel excavation, resulting in deformable body with obvious outline of basically transfixed cracks (Fig. 5).

To ensure the tunnel safety, a displacement monitoring system was installed within the ancient landslide of zone I in January 2015 before tunnel excavation on the base of the borehole-revealed sliding body shape and measured ground surface deformation as shown in Fig. 2. This system includes five ground monitoring sites, namely, JC01, JC02, JC05, JC06 and JC08,

and three inclinometer sites, namely, JC02, JC06 and JC08. The inclinometers, with 60m depth in JC02, 75m depth in JC06, and 75m depth in JC08, were applied to observe the displacement variation with depth, with one monitoring point every 1m depth. The measurement of vertical and horizontal displacements was conducted every 24h interval with GPS.

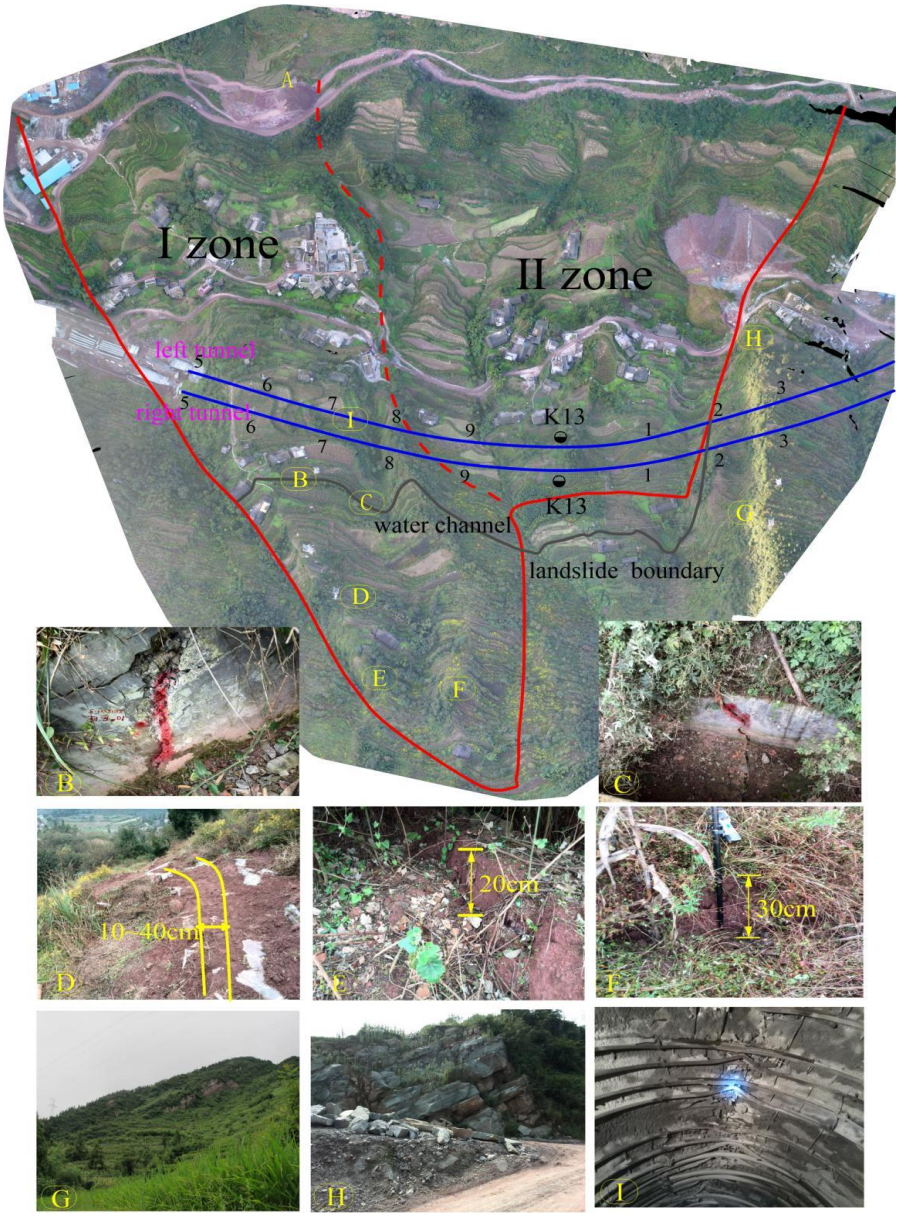

Fig.5 Damage to tunnel and slope. (A) damage scope; (B) crack in the aqueduct; (C) deformation of landslide in the western boundary; (D) settlement crack behind landslide; (E) Eastern boundary of the landslide; (F) bedrock of the landslide in eastern boundary; (G) deformation of the left tunnel vault

The measured data were plotted in Fig. 6, which indicates that the maximum displacement on the ground surface occurred at JC08 and was about 85mm. The maximum displacements on the ground surface were 6mm at JC09, 4mm at JC10 and 5mm at JC18. Zone II and the lower part of zone I had small displacement, indicating that most displacement occurred in the middle and upper part of zone I. The displacements before October 15, 2015 increased gradually, generally smaller than 19 mm, partly up to 34 mm near the ground surface. Subsequently, the displacement of tunnel was basically controlled with timely reinforcement. On October 15, 2015, however, the deep displacement increased sharply, with 35-51mm, 45-64 mm and 60-74 mm at JC02, JC06 and JC08, respectively. The displacements increased in a gradual way from top to bottom. The two potential sliding surfaces were verified by the two abrupt changes in JC08. After October 15, 2015, the measurement was terminated because the landslide sliding damaged the three inclinometers. According to the shape of the displacement curve, depth of the slip surface could be detected, 31m at JC02, 46m at JC06, 55m at JC06. The position of the sliding surface determined by deformation monitoring is consistent with the position revealed in the engineering geological survey profile.

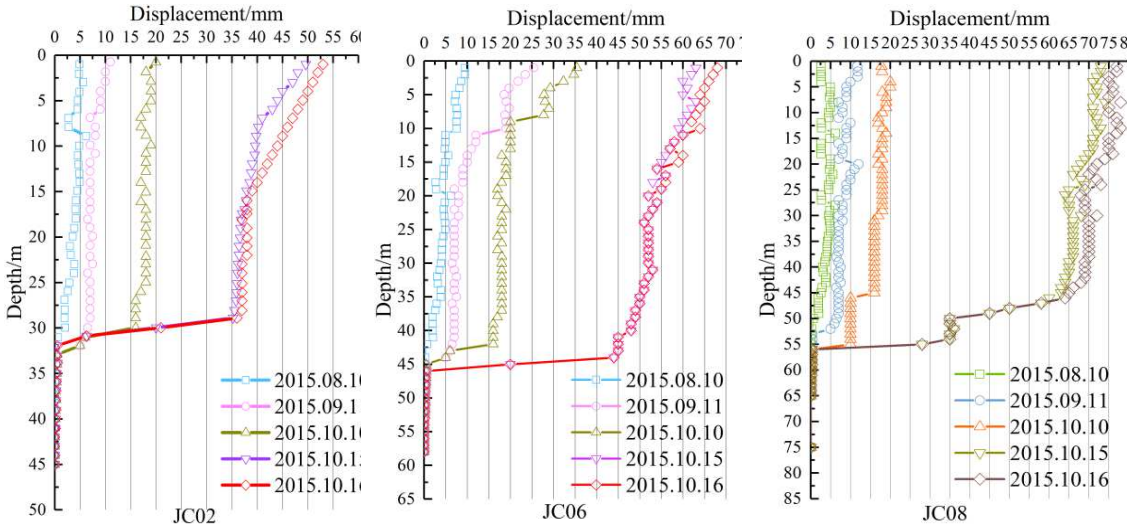

Fig. 6 Curves for measured displacement at different depths in various periods

237 **4.2 Tunnel deformation and monitoring**

238 The landslide can cause the tunnel to be subject to two kinds of deformation (Poisel et al.,
239 2009; Tao and Zhou, 2007; Wei et al., 2019), one is the plunging, longitudinal bending and overall
240 movement due to landslide pushing and creeping forces, and the other is the squeezing
241 deformation by landslide creeping.

242 On October 15, 2015, the excavation and secondary lining of right tunnel had been finished,
243 and the left tunnel entrance was constructed at ZK12+644 and the left tunnel exit at ZK12+682.
244 On the same day, oblique cracks were found within the tunnel bottom and secondary lining in the
245 ZK12+829 to +817 section, and remarkable deformation was observed in the primary support
246 structure in ZK12+799 to +766 section, which resulted in twist break and deformation in the
247 tunnel top. The right wall deformed greatly beyond the limit by up to 65-69cm, and some concrete
248 dropped from primary support on the tunnel top. Some longitudinal and connected cracks, up to
249 3mm wide, were observed on the top right and bottom left of the right tunnel in K12+540 to +719
250 section. By the middle of December 2015, great deformation and many cracks were observed in
251 the right tunnel of K12+505 to +719 section, with some minor cracks in K12+719 to +799 section.
252 At the same time, cracks occurred in the left tunnel of ZK12+505 to +849 section, especially
253 abundant in ZK12+800 to +767 section.

254 Some monitoring gauges were installed immediately after the severe tunnel deformation, as
255 shown in Fig. 7, with displacement gauges at K12+560, K12+600 and K12+722, strain gauges for
256 temporary oblique support at K12+560, K12+580, K12+600 and K12+620, steel bar stress gauges
257 at K12+538, and concrete stress gauges for secondary lining at K12+554. Type and resolution of
258 the monitoring gauges were shown in Table 1. The tunnel displacement curves are shown in Fig. 8,

stress curves of temporary oblique support in Fig. 9, stress curves of lining steel bars in Fig. 10, and stress curves of secondary lining concrete at K12+554 in Fig. 11. All the gauges began successively to work from the middle of November, 2015. The tunnel displacement at K12+720 kept stable since December 12, 2015, with a cumulative displacement of 6.19mm, and the displacement at K12+560 and K12+600 stayed stable since January 2, 2016, with a cumulative displacement of about 5.70mm. The stresses of oblique supports at K12+560, K12+580 and K12+620 within ancient landslide were generally stable, only with a short-term sharp increase at K12+600 on December 13, 2015 and then a tendency to about 60MPa. Since December 2, 2015, the steel bar at the right of lining was obviously under tension but basically stable, without any significant increase in stress. The right side wall of lining was under tension of about 2MPa, and the tunnel top and left side wall were under compression of about 4MPa. The measured data above indicated that the tunnel within the ancient landslide was generally stable since January 3, 2016.

Table 1 Type and resolution of the monitoring gauges

monitoring equipment	Type specification	Basic parameters
displacement gauges	JSS30A	measurement range 0.5～20m, division ratio 0.01mm, measurement accuracy 0.06mm, size 410mm×100mm×35mm, ambient temperature 0～ 40 degrees.
Supporting strain gauge	9000 vibrating string type	measurement range 0～3000με, Sensitivity 1με, frequency range450～1000HZ, size 170mm×265mm, ambient temperature-20～80 degrees.
concrete stress meter	SZZX-A150 vibrating string type	measurement range-1500με～1500με, Sensitivity 1με, measuring mark distance size 157mm, ambient temperature--20～125 degrees.
steel stress meter	9011 vibrating string type	measurement range-3000kg/cm^2～3000 kg/cm^2, Sensitivity 0.025%FS, size750mm, ambient temperature--20～80degrees.

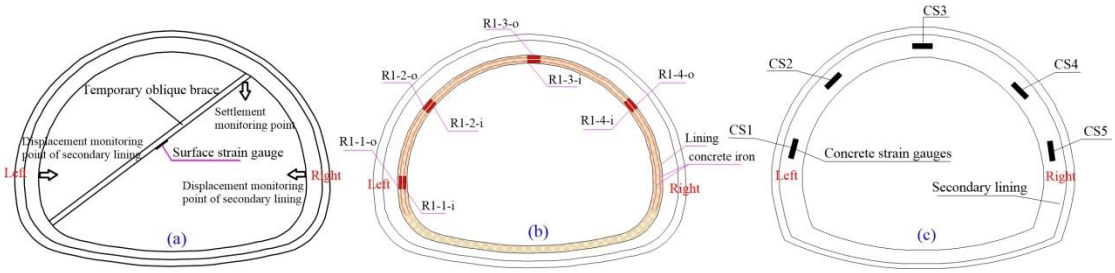

273

274 **Fig. 7 Monitoring gauges for tunnel. (a) displacement of secondary lining of right tunnel and stress of**

275 **temporary oblique support; (b) stress of steel bar in lining; (c) stress of concrete of secondary lining**

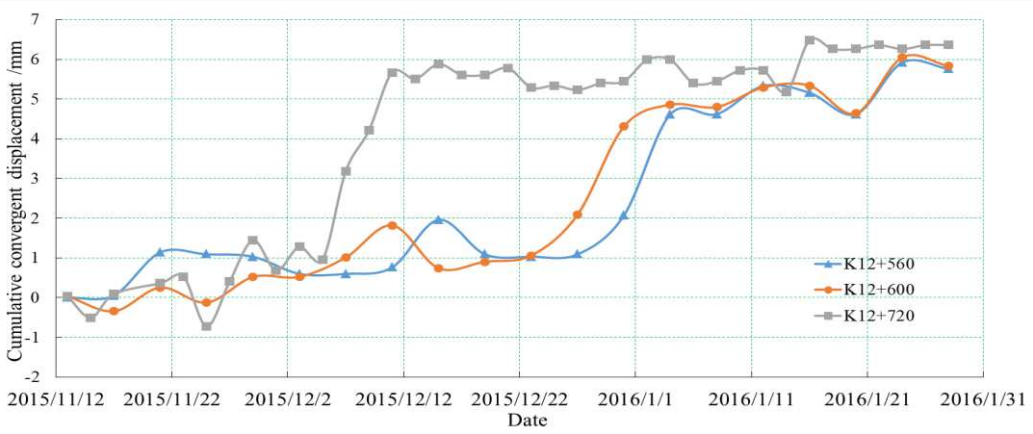

276

277 **Fig.8 Displacement curves for tunnel within ancient landslide**

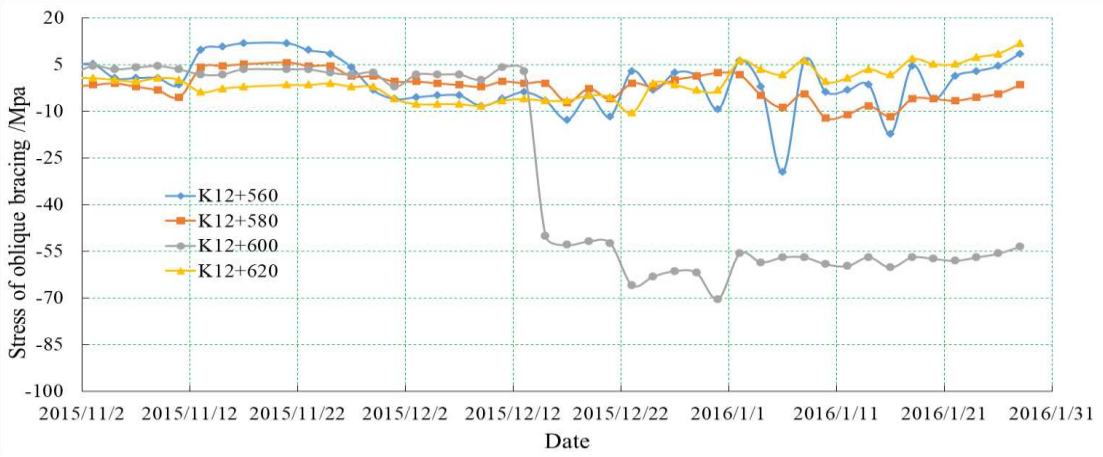

278

279 **Fig.9 Stress curves for temporary oblique support**

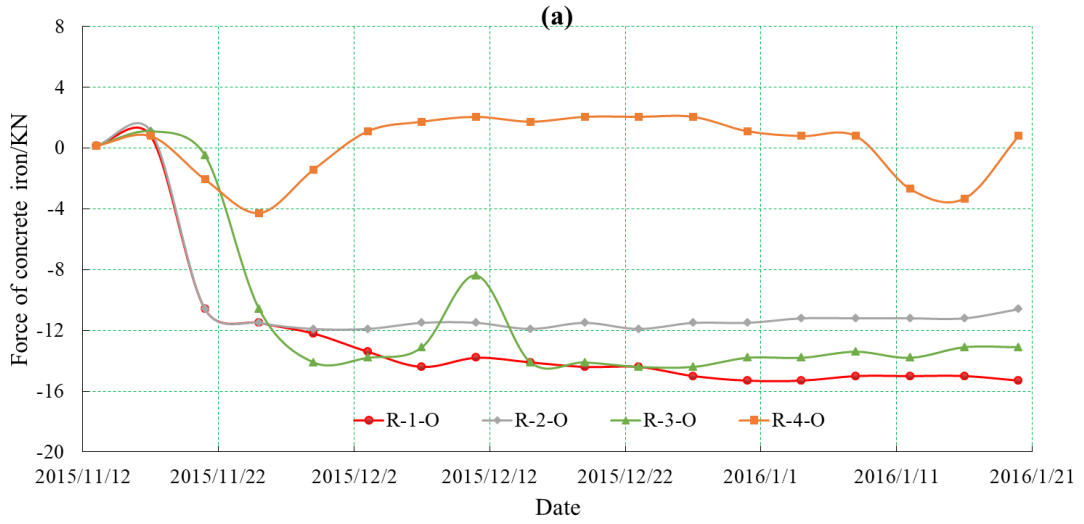

280

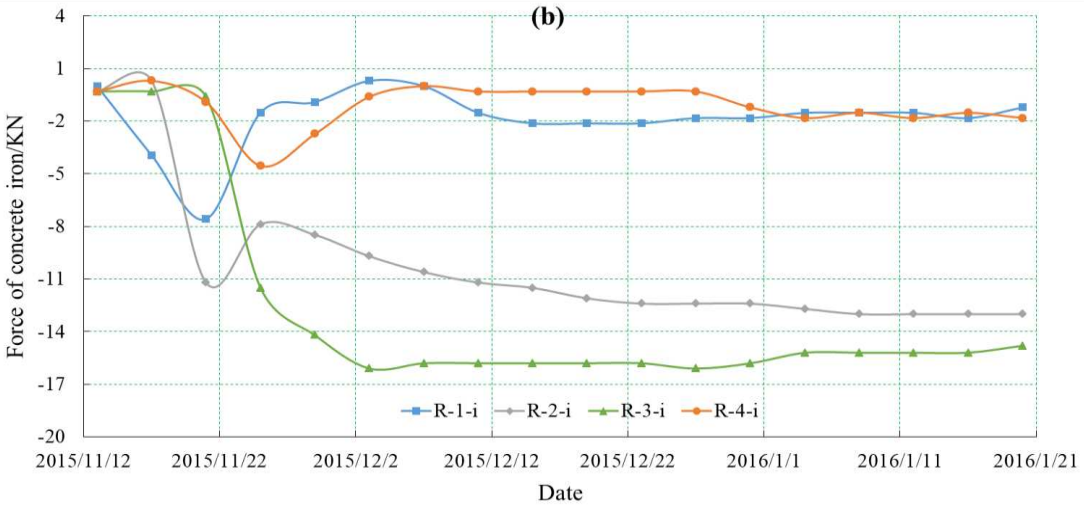

281

282 **Fig.10 Stress curves of steel bar at K12+538. (a) in inner lining; (b) in outer lining.**

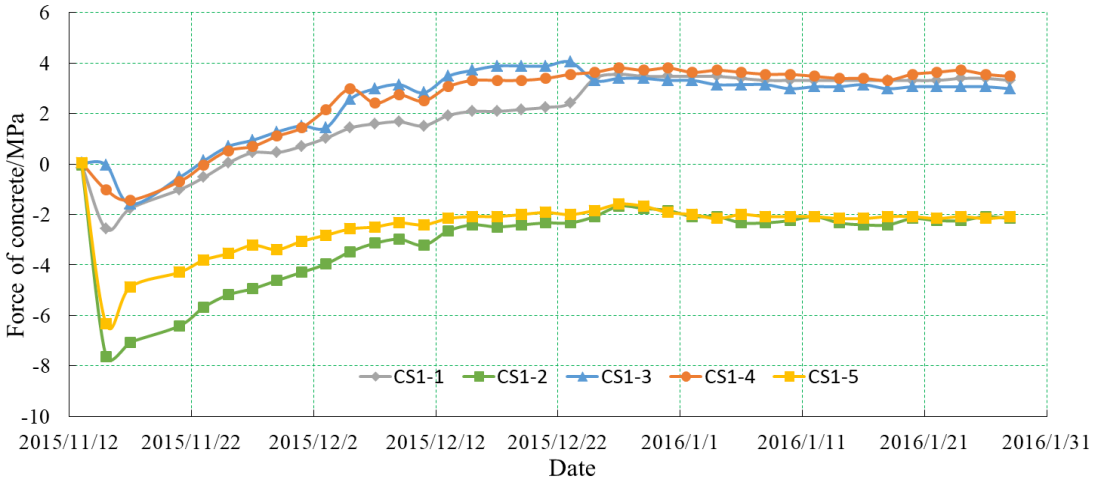

283

284 **Fig.11 Stress curves for concrete of secondary lining at K12+554**

5. Numerical analysis to landslide induced by tunnel excavation

5.1 Model and parameters

Engineering geological analysis, geological survey, field monitoring and numerical simulation are often used to study the slope failure mechanism and predict the landslide movement. It is difficult to conduct accurate numerical simulation for practical application because of the spatial & temporal variation of strata and geological structure complexity (Marcato et al., 2012), but increasing improvement in the numerical simulation have been achieved due to much quantitative analysis to landslide deformation, movement and risk (Chen and Wu, 2018; Han et al., 2014; Jacquemart, 2017; Jiao, 2013; Kalenchuk et al., 2009; Zhang et al., 2015). In addition, numerical calculation parameters may be optimized by abundant data from borehole, field investigation, laboratory tests, and on-site monitoring, which causes the numerical simulation more accuracy and applicable (Pirulli et al., 2011; Poisel et al., 2009). Generally, too much simplification in geological structures during numerical modelling may reduce the simulation precision, and thus establishing accurate and complex 3D numerical model is the key to reasonable analysis to landslide stability. Combining on-site investigation data, geological structures, terrain feature and hydrological conditions with deformation monitoring data, the 3D numerical model of Jimei landslide was developed including sliding body, sliding belt, tunnel lining, and bedrock, as shown in Fig. 12. The FLAC^{3D} program, which can well simulate the interaction between rock/soil and structures, was used to analyze the stress and deformation of landslide.

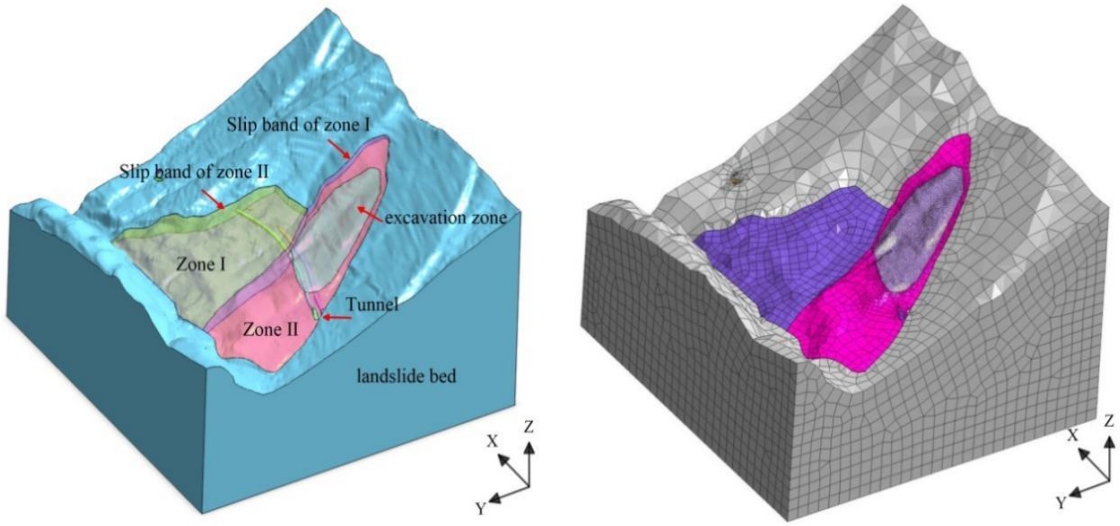

Fig.12 3D numerical model of landslide and tunnel

For the initial stress condition, the tectonic stresses were ignored, and only gravity-induced stresses were considered. For the boundary conditions, the model bottom was fixed in the vertical direction, and the sides are fixed horizontally and vertically. The elastic-plastic constitutive relation and Mohr-Coulomb failure criterion were applied for rock/soil, and the entity elements were used for the primary and the secondary linings with linearly elastic model.

The model parameters should be determined in an appropriate way. The Poisson's ratio, unit weight and elastic modulus were obtained by laboratory tests using samples from each borehole (Fig.1). The soil samples were adopted every one meter in depth from each borehole. The strength parameters were determined by back analysis utilizing uniform design, RBF neural network model (Wang et al., 2013), and measured displacement data about landslide surface. Table 2 lists the comparison between monitoring data and back analysis based results, indicating that all the errors of monitoring points are less than 5% except that the errors of JC01 X displacement, JC06 Z displacement and JC08 Z displacement are greater than 5%, which means that the parameters from back analysis are appropriate. Table 3 lists the geotechnical parameters for numerical calculation.

Table 2 Comparison between field monitoring data and back-analysis calculation results

	JC02 displacement		JC06 displacement		JC08 displacement	
	(Y/mm)	(Z/mm)	(Y/mm)	(Z/mm)	(Y/mm)	(Z/mm)
Measured data	54.0	36.2	68.0	12.8	85.0	21.6
Calculated results	52.6	35.5	65.6	11.9	81.3	20.8
Errors	2.5%	1.9%	3.5%	7.0%	4.35%	3.7%

Note: Y and Z represent the horizontal displacement and vertical displacement, respectively.

Table 3 Numerical model parameters

Location	Elasticity modulus (E/Pa)	Poisson's ratio (μ)	Cohesion (C/kPa)	Internal friction angle (°)	Unit weight (kN/m³)
sliding belt	4E+07	0.35	30	19	2320
sliding body	7.0E+07	0.33	36	28	2350
bedrock	5.0E+09	0.26	6000	42	2640
tunnel lining	9.0E+09	0.20	—	—	2500

5.2 Simulation results and analysis

Based on the 3D numerical calculation, the stress and deformation of the tunnel and sliding body after tunnel reinforcement and soil removal was achieved. The Y-direction displacement contour after reinforcement of tunnel is shown in Fig. 13, indicating that the sliding body deformation basically occurs in the region over the tunnel, and changes gradually from landslide tail to front in a decreasing way. The displacement contour (Fig. 14) and shear strain increment contour (Fig. 15) are plotted along some typical sections (Fig. 13) to clearly observe the stress & deformation within the slope. Fig. 14 suggests that the ancient landslide will fail again due to tunnel excavation, and the deformation feature by numerical simulation is similar to on-site investigation results of gradual deformation decreasing from tail to front. Additionally, great

displacement occurs on the top and right side wall of let tunnel, with terrible inward invasion of right wall. Fig. 15 indicates the distribution of maximum shear strain within the slope, with maximum value of about 0.62, and the sliding surface was not thoroughly developed.

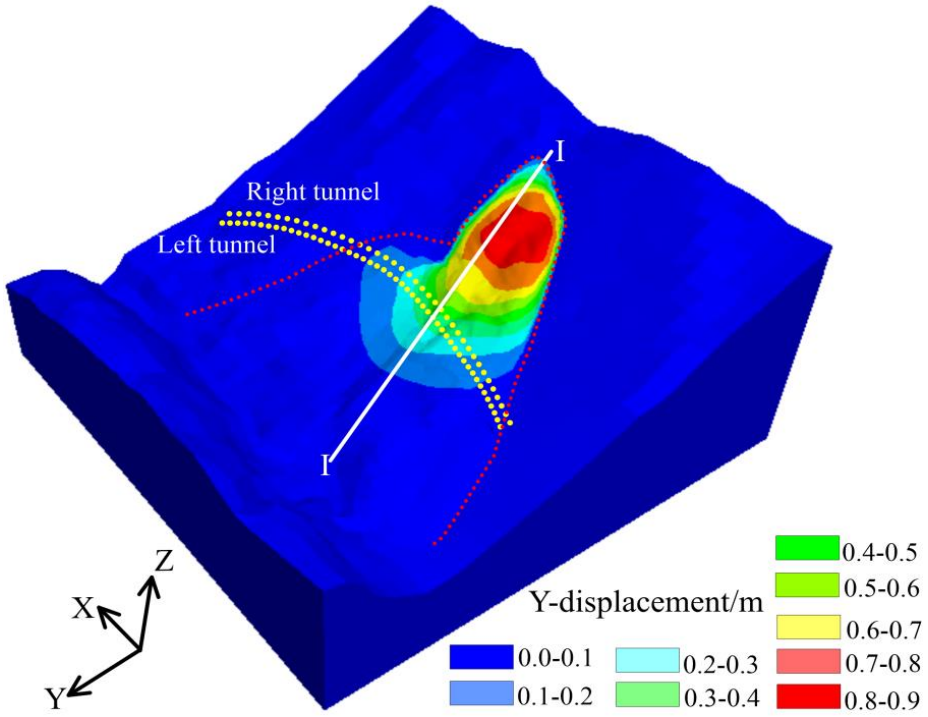

Fig.13 Y-**displacement contour after completion of tunnel excavation (unit: m)**

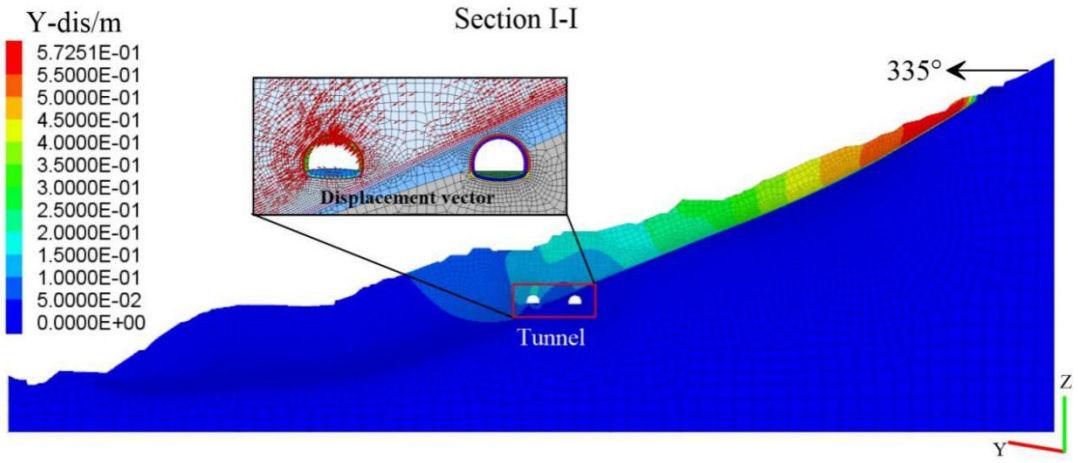

Fig.14 Y-d**isplacement contour after tunnel excavation for typical section (I-I) (unit: m)**

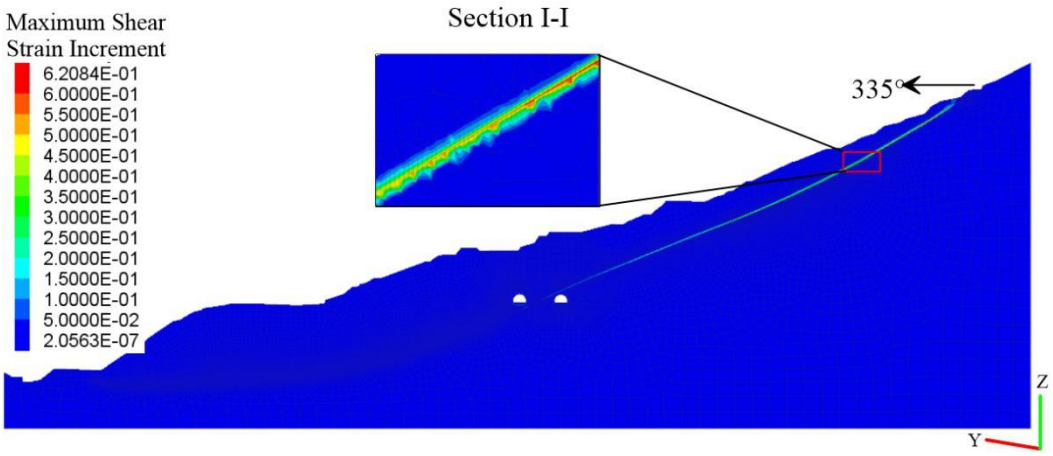

341

342 **Fig.15 Maximum shear strain increment contour along section (I-I) after tunnel excavation**

343 The displacement and stress contours are shown in Figs. 16 and 17. Most displacement
344 occurs in the medium and lower sections of the sliding body, with maximum displacement of
345 around 23.60mm. The maximum displacement of tunnel is at the top of left tunnel, approximately
346 5.8mm. After soil removal, the maximum shear strain increment of the sliding body is very small,
347 with maximum value of only 0.01. The strength reduction method was applied to analyze the
348 stability of landslide after soil removal, and the calculated safety factor is 1.32, indicating that the
349 tunnel will be generally stable by means of concrete lining.

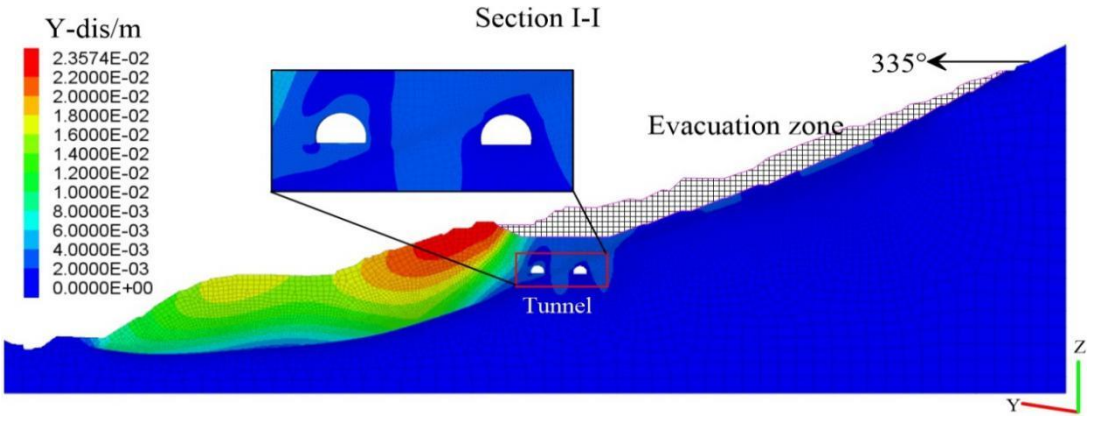

350

351 **Fig.16** Y-**displacement contour after soil removal along section I-I (unit: m)**

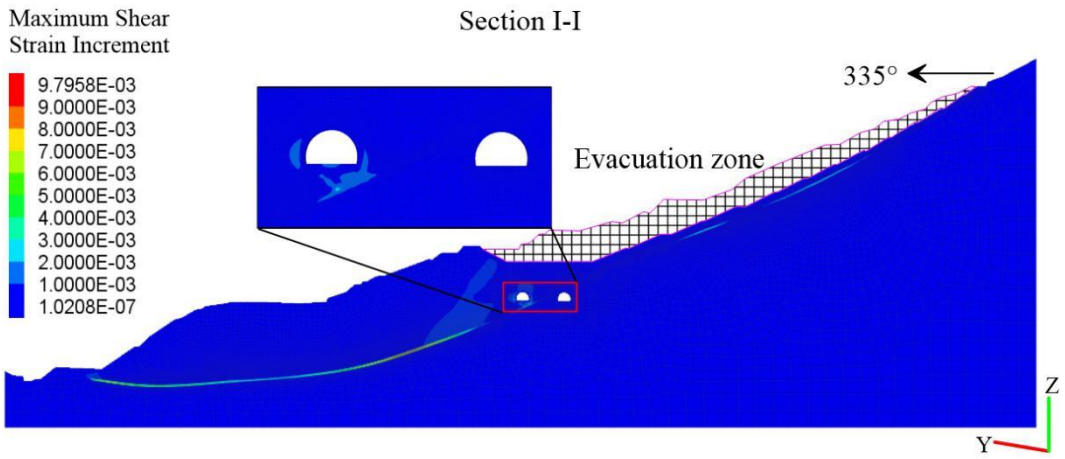

Fig.17 Maximum shear strain increment contour after soil removal along section I-I

6. Discussion

6.1 Prevention measures for landslide and tunnel

Increasing anti-slide force by anti-slide pile, slope-toe backfilling, retaining wall, and anchor cable and and/or reducing sliding force by drainage and slope-top unloading are two major measures for landslide prevention ((Brunet et al., 2017; Di Maio et al., 2010; Segoni et al., 2018; Wang et al., 2019). Jimei tunnel, as a key part of highway, has a direct effect on the commence of the highway operation, and thus the time-saving and reliable measures should be used first if the construction and operation safety of tunnel is guaranteed.

According to on-site survey and numerical simulation results, the ancient landslide in zone II are generally stable, without tunnel deformation and ground cracking, and thus no treatment is needed for landslide in this zone, only with monitoring hereafter. The ancient landslide in zone I is also generally stable, but the left tunnel is completely in the sliding body and the right tunnel is just across the sliding surface, which resulted in the damage to right tunnel and upper slope. The depth of the tunnel is greater than 60m, the adjacent strata affected is averagely 35-40m deep, and thus it is not feasible to use the anti-slide piles as tunnel reinforcement. In addition, the anti-slide

piles would need very high cost and larger length of up to 80m. However, the lower landslide is thick and upper landslide is thin, and hence it is suitable to stabilize the landslide by removing soil from upper part into slope toe and conducting some reinforcement at lower part.

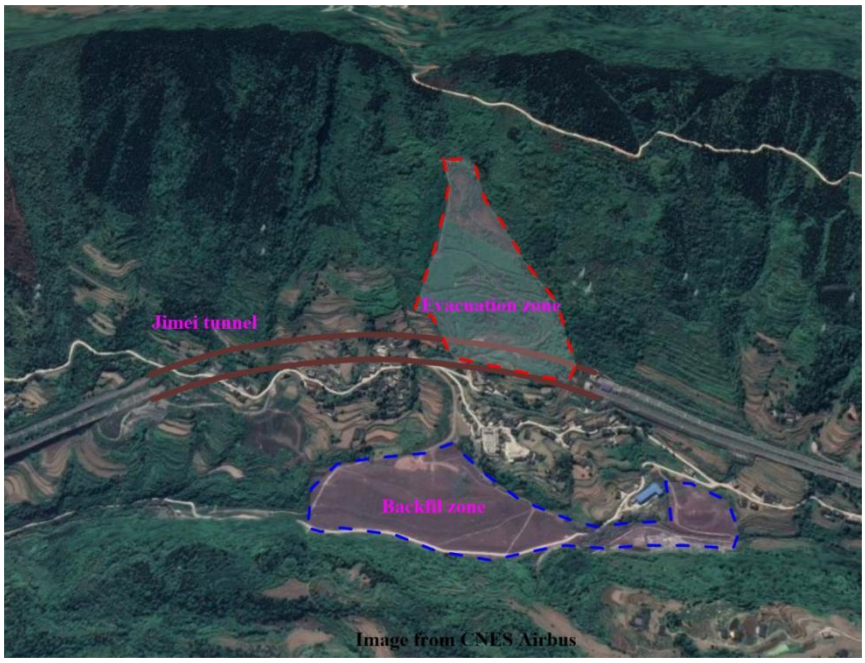

Fig.18 Bird view of construction site after soil removal

6.2 landslide and tunnel monitoring system

A monitoring system was established to measure the stress and displacement of landslide and tunnel during the operation period of Jimei tunnel. The content and purpose of the system is described as follows.

(1) The stress and strain of surrounding rock and tunnel structure will be measured during tunnel operation period.

(2) According to monitoring data, the stability and safety of tunnel and landslide will be analyzed, and the range, speed and tendency of deformation for landslide and tunnel will be also evaluated to safeguard the tunnel operation.

(3) The tunnel deformation limit will be judged as early as possible to provide early warning

to administration for determining the subsequent safety measures.

The monitoring data measured from October 2016 to March 2020 show that the displacement at various depths are generally stable, and the change in stresses of steel bar, concrete and support is little, indicating the treatment applied is successful. Thus, the anti-slide piles were not installed, saving about seven million US$. There are few successful treatment cases of such tunnel-landslide systems under complex conditions, so the analysis and design in this paper can provide some beneficial reference to similar projects.

7. Conclusions

An ancient landslide was reactivated in October 2015 after the excavation of Jimei tunnel in Sichuan Province, China, which triggered many severe geological problems such as tunnel deformation, ground surface cracks and supporting structure damage. Such slope failure may have great threat to residents and facilities, and sharply increase the construction cost. Several methods were used to analyze the interaction between Jimei tunnel and the ancient landslide, and the proposed reinforcement was evaluated in this paper.

At first, the composition and distribution of the ancient landslide was analyzed based on the UAV aerial photography, geological prospecting and field geological survey. Secondly, the parameters of the sliding zone and sliding body were determined with back analysis according to the monitoring data about the surface deformation. Finally, the landslide failure mechanism due to tunnel excavation was discussed by 3D numerical simulation, and the evaluation on the effect of proposed reinforcement was carried out.

The borehole data show that the Jimei landslide, as an ancient landslide, is more than 50m thick on average, with over 11 million m^3 in volume, being the giant deep-seated landslide. The

406 sliding body consists basically of block stone and gravel, and the slope failure generally resulted
407 from the tunnel excavation through the sliding belt. Most displacement of the sliding body mainly
408 occurred above the tunnel because the potential sliding surface under the tunnel is gentle and the
409 deep-seated sliding body prevented further sliding. In addition, the range and value of overall
410 displacement of the sliding body by back analysis match well the field survey and measured data.
411 In view of tunnel construction period, sliding body thickness and deformation characteristics,
412 some soil above the tunnel in zone I was suggested to be removed. Numerical simulation results
413 show that the tunnel and sliding body will be subject to small displacements and keep stable after
414 soil is removed. The monitoring data measured during tunnel operation period testified the success
415 of the treatment, and this paper may present a beneficial reference to similar projects.

416 # Acknowledgments

417 The authors would like to acknowledge the National Key Research and Development
418 Program (Grant No. 2019YFC1509704), High-level Talent Project of North China University of
419 Water Resource and Electric Power (Grant No.201518), National Natural Science Foundation of
420 China (Grant No. U1704243), and Levee Safety and Disaster Prevention Engineering Research
421 Center of Ministry of Water Resources.

422

423 # References

424 Bandini, A., P. Berry, and D. Boldini, 2015, Tunnelling-induced landslides: The Val di Sambro tunnel
425 case study: Engineering Geology, v. 196, p. 71-87. https://doi:10.1016/j.enggeo.2015.07.001

426 Bayer, B., A. Simoni, D. Schmidt, and L. Bertello, 2017, Using advanced InSAR techniques to monitor
427 landslide deformations induced by tunneling in the Northern Apennines, Italy: Engineering
428 Geology, v. 226, p. 20-32.
429 Brunet, M., L. Moretti, A. Le Friant, A. Mangeney, E. D. Fernández Nieto, and F. Bouchut, 2017,
430 Numerical simulation of the 30–45 ka debris avalanche flow of Montagne Pelée volcano,
431 Martinique: from volcano flank collapse to submarine emplacement: Natural Hazards, v. 87, p.
432 1189-1222.
433 Chen, K.-T., and J.-H. Wu, 2018, Simulating the failure process of the Xinmo landslide using
434 discontinuous deformation analysis: Engineering Geology, v. 239, p. 269-281.
435 https://doi:10.1016/j.enggeo.2018.04.002
436 De-pei, Z., M. A. Jian-qiang, Z. Lu-xing, and M. Hui-ming, 2002, Relationship between tunnel
437 deformation with slope disasters and its prediction model: journal of The China Railway
438 Society, v. 24, p. 81-86.
439 Di Maio, C., R. Vassallo, M. Vallario, S. Pascale, and F. Sdao, 2010, Structure and kinematics of a
440 landslide in a complex clayey formation of the Italian Southern Apennines: Engineering
441 Geology, v. 116, p. 311-322.
442 Gu, D. M., D. Huang, W. D. Yang, J. L. Zhu, and G. Y. Fu, 2017, Understanding the triggering
443 mechanism and possible kinematic evolution of a reactivated landslide in the Three Gorges
444 Reservoir: Landslides, v. 14, p. 2073-2087.
445 Han, Z., G. Chen, Y. Li, L. Xu, L. Zheng, and Y. Zhang, 2014, A new approach for analyzing the
446 velocity distribution of debris flows at typical cross-sections: Natural Hazards, v. 74, p.
447 2053-2070.

448 Itasca Consulting Group Inc, 2005, FLAC3D: fast Lagrangian analysis of continua in 3 dimensions,
449 user manual (version 3.0). Itasca Consulting Group Inc., Minneapolis, Minnesota
450 Jacquemart, M., L. Meier, C. Graf, and F. Morsdorf, 2017, 3D dynamics of debris flows quantified at
451 sub-second intervals from laser profiles: Natural Hazards, v. 89, p. 785-800.
452 Jian-qiang, M., and Z. De-pei, 2002, Deformation Analysis for Landslide-Tunnel Interaction: journal of
453 Southwest Jiaotong University v. 37, p. 371-376.
454 Jiao, Y.-Y., Z.-H. Wang, X.-Z. Wang, A. C. Adoko, and Z.-X. Yang, 2013, Stability assessment of an
455 ancient landslide crossed by two coal mine tunnels: Engineering Geology, v. 159, p. 36-44.
456 https://doi:10.1016/j.enggeo.2013.03.021
457 Kalenchuk, K. S., D. J. Hutchinson, and M. S. Diederichs, 2009, Application of spatial prediction
458 techniques to defining three-dimensional landslide shear surface geometry: Landslides, v. 6, p.
459 321-333. https://doi:10.1007/s10346-009-0168-1
460 Karakus, M., and R. J. Fowell, 2005, Back analysis for tunnelling induced ground movements and
461 stress redistribution: Tunnelling and Underground Space Technology, v. 20, p. 514-524.
462 Kaya, A., A. Akgün, K. Karaman, and F. Bulut, 2015, Understanding the mechanism of slope failure on
463 a nearby highway tunnel route by different slope stability analysis methods: a case from NE
464 Turkey: Bulletin of Engineering Geology and the Environment, v. 75, p. 945-958.
465 https://doi:10.1007/s10064-015-0770-5
466 Komu, M. P., U. Guney, T. E. Kilickaya, and C. Gokceoglu, 2019, Using 3D Numerical Analysis for
467 the Assessment of Tunnel–Landslide Relationship: Bahce–Nurdag Tunnel (South of Turkey):
468 Geotechnical and Geological Engineering, v. 38, p. 1237-1254.

469 Konagai, K., M. Numada, A. Zafeirakos, J. Johansson, A. Sadr, and T. Katagiri, 2005, An example of
470 landslide-inflicted damage to tunnel in the 2004 Mid-Niigata Prefecture earthquake:
471 Landslides, v. 2, p. 159-163. https://doi:10.1007/s10346-005-0057-1
472 Liu, H., j. Shen, W. Wei, and Z. Guan, 2012, Geological Problems and Treatment Measures For
473 Highway Tunnel Through Ancient Landslide: Journal of Engineering Geology, v. 20, p.
474 540-547.
475 Ma, H., 2003, DISCUSSION ON PROBLEMS OF SLOPE DISASTER AND TUNNEL
476 DEFORMATION: Chinese Journal of Rock Mechanics and Engineering, v. 22, p. 2719-2724.
477 Ma, h., and H. Wu, 2016, Progress and Expectation of Rearch on Tunnel-Landslide System: Chinese
478 Journal of Underground Space and Engineering, v. 12, p. 522-531.
479 Minardo, A., E. Catalano, A. Coscetta, G. Zeni, L. Zhang, C. Di Maio, R. Vassallo, R. Coviello, G.
480 Macchia, L. Picarelli, and L. Zeni, 2018, Distributed Fiber Optic Sensors for the Monitoring
481 of a Tunnel Crossing a Landslide: Remote Sensing, v. 10, p. 1291.
482 https://doi:10.3390/rs10081291
483 Mishra, Mayank & Vassallo, Roberto & Santarsiero, Giuseppe & Masi, Angelo. (2017).
484 Landslide-pile-tunnel interaction by 2D and 3D finite element modelling.
485 10.7712/120117.5752.17314.
486 Pánek, T., J. Hradecký, V. Smolková, and K. Šilhán, 2008, Giant ancient landslide in the Alma water
487 gap (Crimean Mountains, Ukraine): notes to the predisposition, structure, and chronology:
488 Landslides, v. 5, p. 367-378.
489 Pirulli, M., A. Colombo, and C. Scavia, 2011, From back-analysis to run-out prediction: a case study in
490 the Western Italian Alps: Landslides, v. 8, p. 159-170. https://doi:10.1007/s10346-010-0248-2

491 Poisel, R., H. Angerer, M. Pöllinger, T. Kalcher, and H. Kittl, 2009, Mechanics and velocity of the
492 Lärchberg–Galgenwald landslide (Austria): Engineering Geology, v. 109, p. 57-66.
493 https://doi:10.1016/j.enggeo.2009.01.002
494 Ruggeri, P., V. Fruzzetti, A. Vita, A. Paternesi, G. Scarpelli, and D. Segato, 2016, Deep-seated landslide
495 triggered by tunnel excavation, p. 1759-1766.
496 Segoni, S., L. Piciullo, and S. L. Gariano, 2018, A review of the recent literature on rainfall thresholds
497 for landslide occurrence: Landslides, v. 15, p. 1483-1501.
498 Tang, H., C. Li, X. Hu, A. Su, L. Wang, Y. Wu, R. Criss, C. Xiong, and Y. Li, 2014, Evolution
499 characteristics of the Huangtupo landslide based on in situ tunneling and monitoring:
500 Landslides, v. 12, p. 511-521.
501 Tao, Z., and D. Zhou, 2003, MODEL TEST ON DEFORMATION MECHANISM OF TUNNEL AT
502 LANDSLIDE SITE: Journal of Engineering Geology, v. 11, p. 323-328.
503 Tao, Z., and D. Zhou, 2007, deformationg law and disaster prediction of tunnel in creep landslide:
504 Journal of Southwest Jiaotong University, v. 42, p. 163-169.
505 Technical Guidance Centre for Geological Disasters, 2019, National Geological Hazard Bulletin.
506 https://www.cgs.gov.cn/gzdt/zsdw/202003/W020200331377465119094.pdf
507 Vassallo, R., M. Mishra, G. Santarsiero, and A. Masi, 2016, Interaction of a Railway Tunnel with a
508 Deep Slow Landslide in Clay Shales: Procedia Earth and Planetary Science, v. 16, p. 15-24.
509 Vassallo, R., M. Mishra, G. Santarsiero, and A. Masi, 2019, Modeling of Landslide–Tunnel Interaction:
510 the Varco d'Izzo Case Study: Geotechnical and Geological Engineering, v. 37, p. 5507-5531.

511 Wang Z., H. Liu, and S. He, 2013, Dynamic deformation monitoring and three-dimensional numerical
512 analysis ofK62 landslide of approach road of A'hai Hydropower Station: Chinese Journal of
513 Geotechnical Engineering, v. 35, p. 94-101.
514 Wei, Z.-l., Y.-q. Shang, H.-y. Sun, H.-d. Xu, and D.-f. Wang, 2019, The effectiveness of a drainage
515 tunnel in increasing the rainfall threshold of a deep-seated landslide: Landslides, v. 16, p.
516 1731-1744.
517 Zhang, Y., J. Yang, and F. Yang, 2015, Field investigation and numerical analysis of landslide induced
518 by tunneling: Engineering Failure Analysis, v. 47, p. 25-33.
519 Zhang, Z.-g., Q.-h. Zhao, C. Xu, and X.-y. Xu, 2017, Interaction analyses between tunnel and landslide
520 in mountain area: Journal of Mountain Science, v. 14, p. 1124-1139.
521 Zhou, S., Z. Tian, H. Di, P. Guo, and L. Fu, 2020, Investigation of a loess-mudstone landslide and the
522 induced structural damage in a high-speed railway tunnel: Bulletin of Engineering Geology
523 and the Environment.

Figures

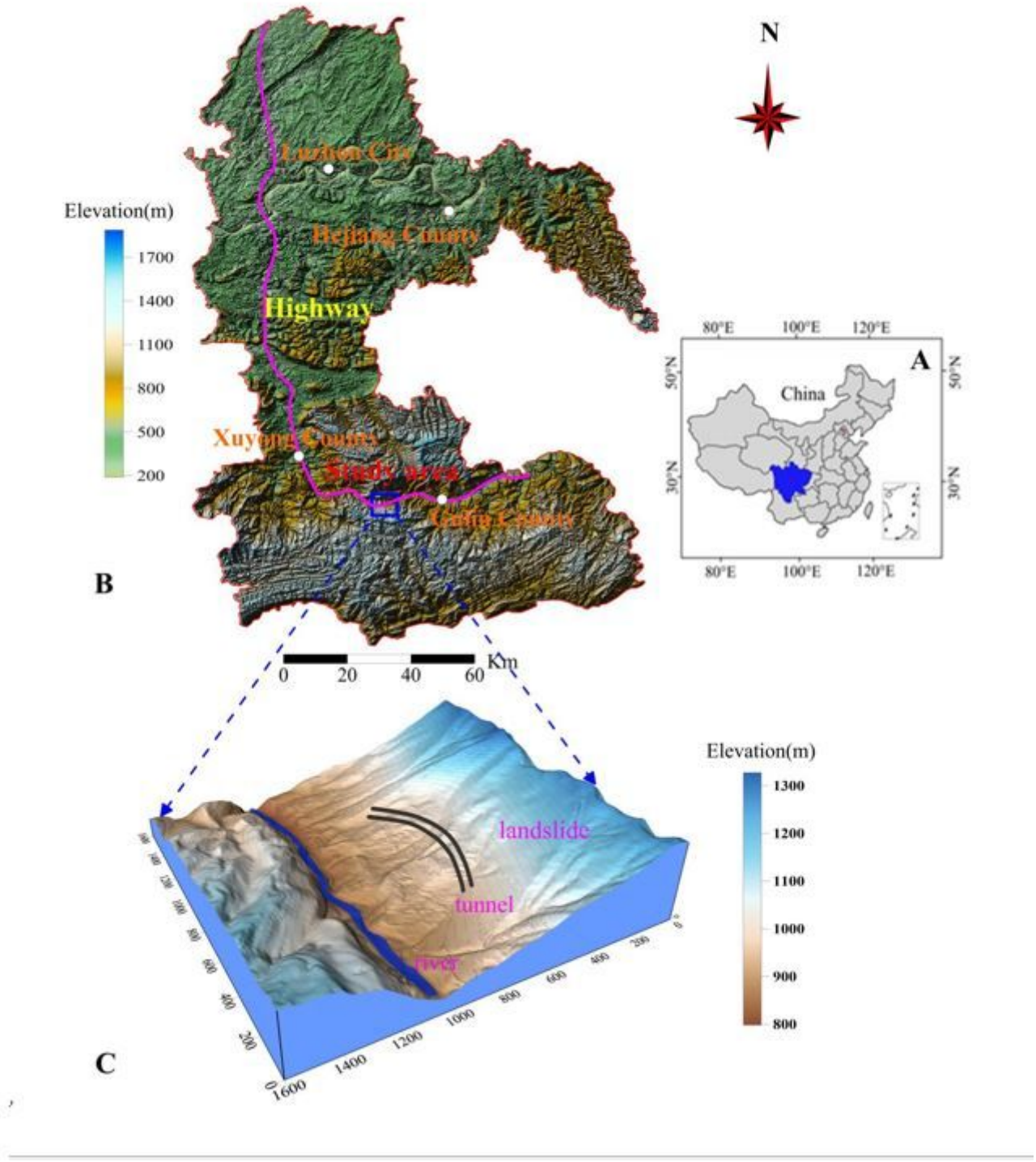

Figure 1

Location of Jimei tunnel. (A) schematic location in china; (B) location of Xuyong-Gulin highway; (C) 3D terrain of Jimi tunnel and landslide. Note: The designations employed and the presentation of the material on this map do not imply the expression of any opinion whatsoever on the part of Research

Square concerning the legal status of any country, territory, city or area or of its authorities, or concerning the delimitation of its frontiers or boundaries. This map has been provided by the authors.

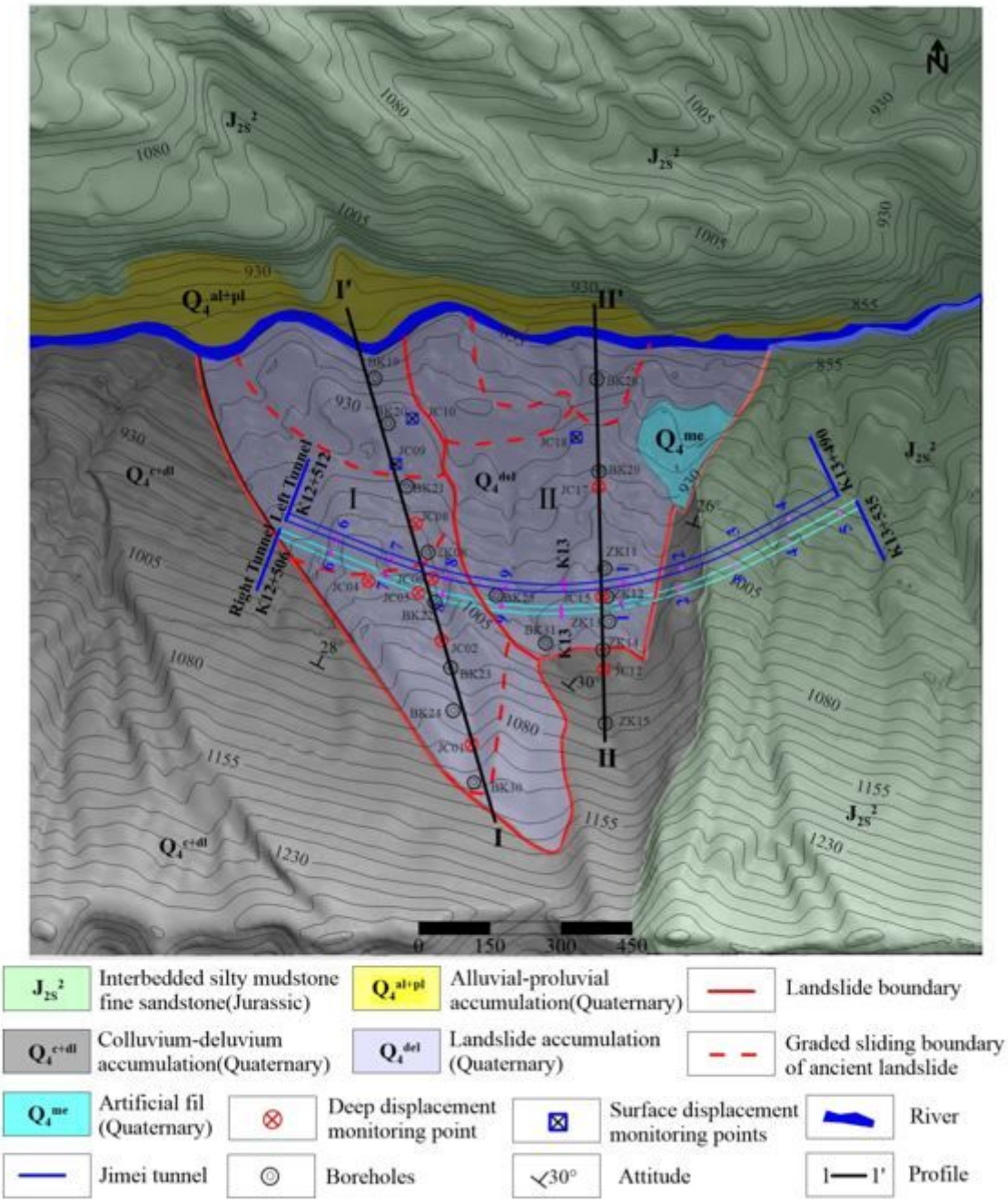

Figure 2

The geological structure of the study area Note: The designations employed and the presentation of the material on this map do not imply the expression of any opinion whatsoever on the part of Research Square concerning the legal status of any country, territory, city or area or of its authorities, or concerning the delimitation of its frontiers or boundaries. This map has been provided by the authors.

Figure 3

Core from (A) borehole BK23; (B) borehole BK14.

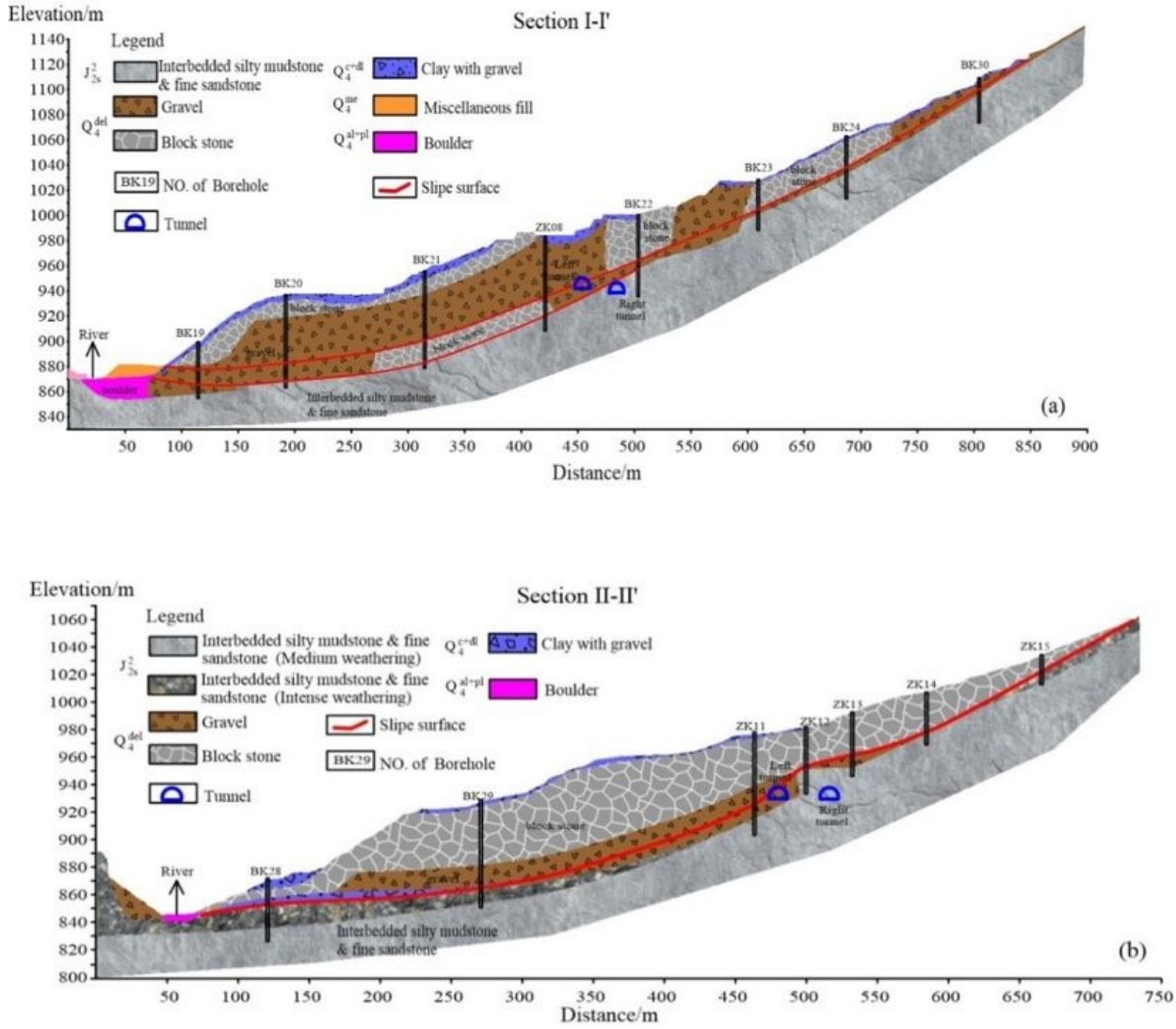

Figure 4

Geological profile of (a) 1-1'; (b) 2-2'.

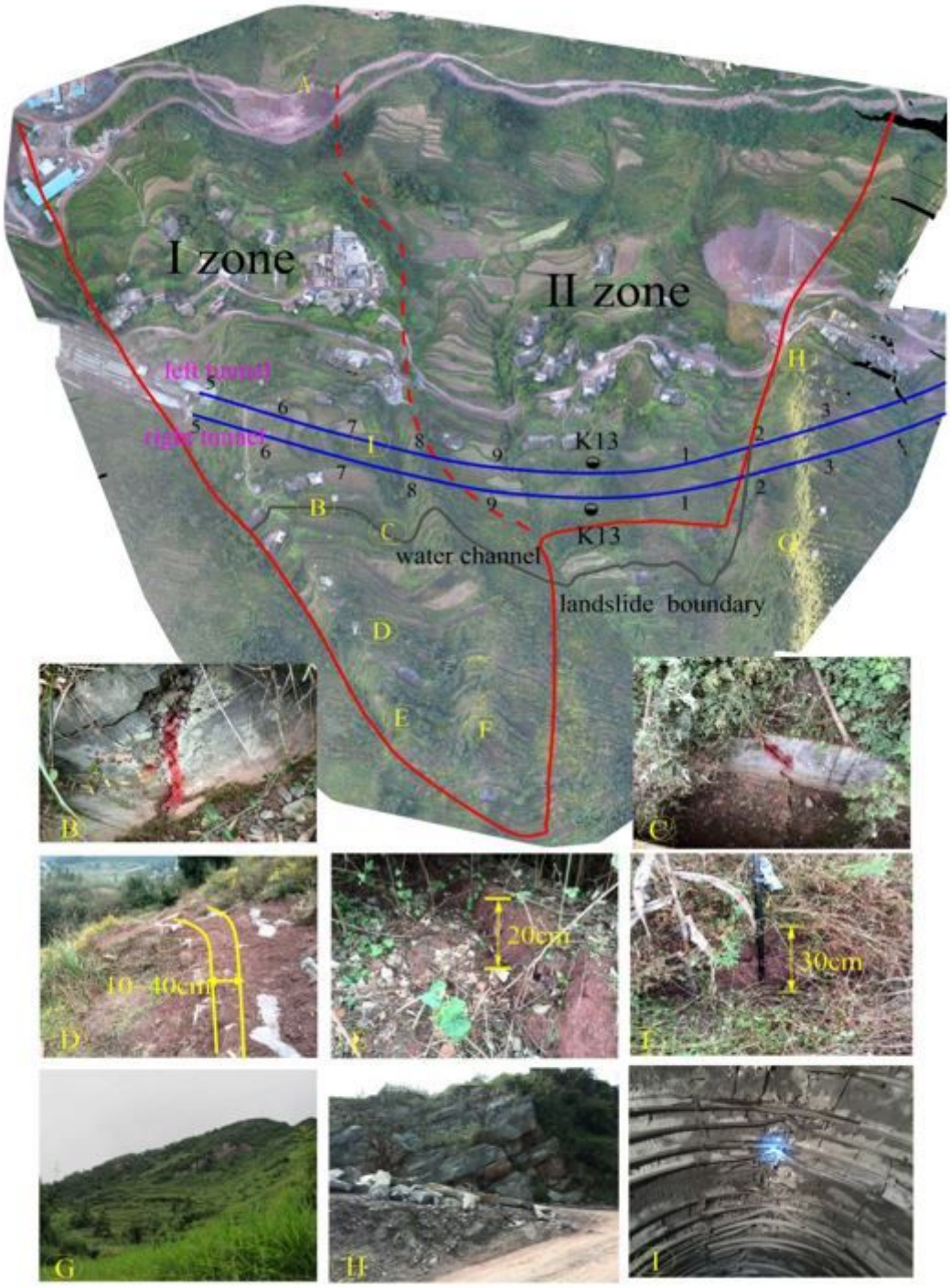

Figure 5

Damage to tunnel and slope. (A) damage scope; (B) crack in the aqueduct; (C) deformation of landslide in the western boundary; (D) settlement crack behind landslide; (E) Eastern boundary of the landslide; (F) bedrock of the landslide in eastern boundary; (G) deformation of the left tunnel vault Note: The designations employed and the presentation of the material on this map do not imply the expression of any opinion whatsoever on the part of Research Square concerning the legal status of any country,

territory, city or area or of its authorities, or concerning the delimitation of its frontiers or boundaries. This map has been provided by the authors.

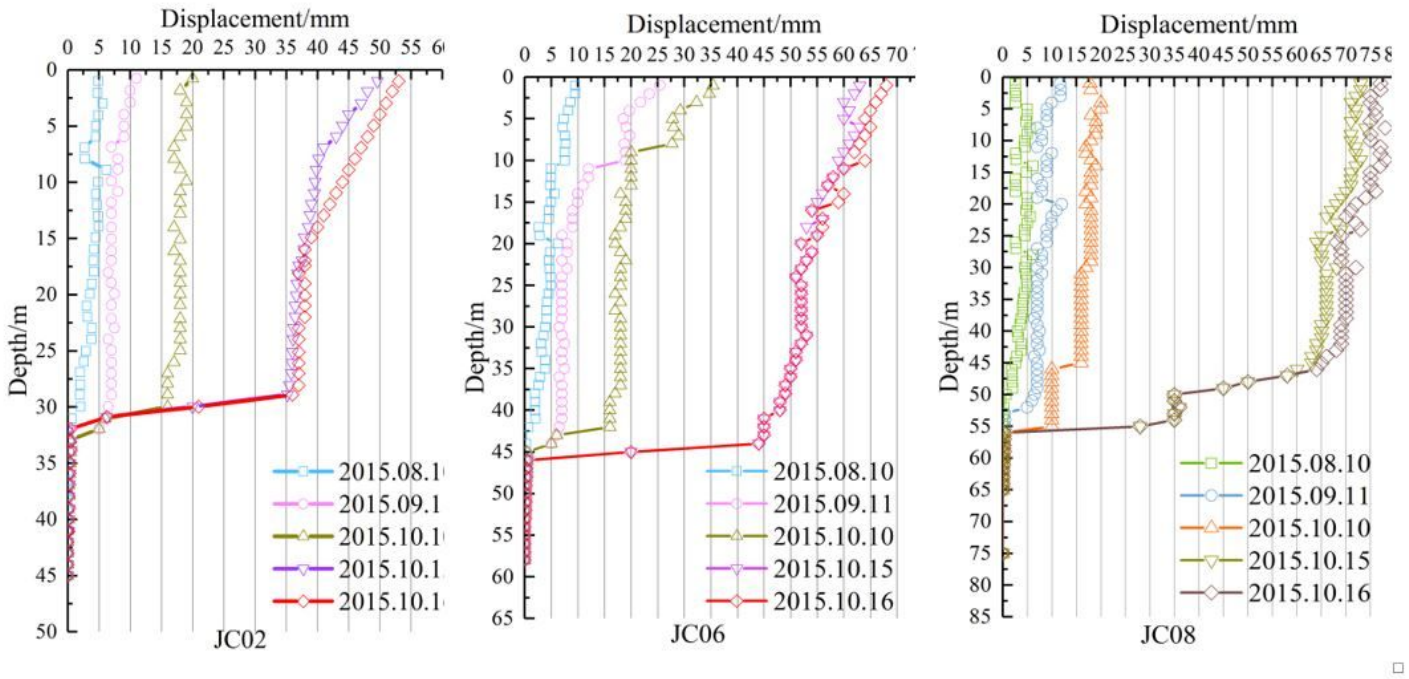

Figure 6

Curves for measured displacement at different depths in various periods

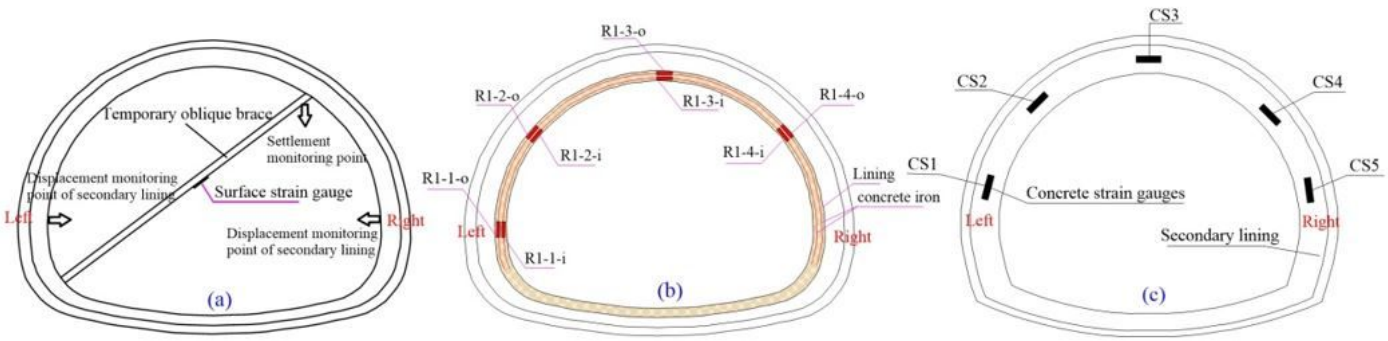

Figure 7

Monitoring gauges for tunnel. (a) displacement of secondary lining of right tunnel and stress of temporary oblique support; (b) stress of steel bar in lining; (c) stress of concrete of secondary lining

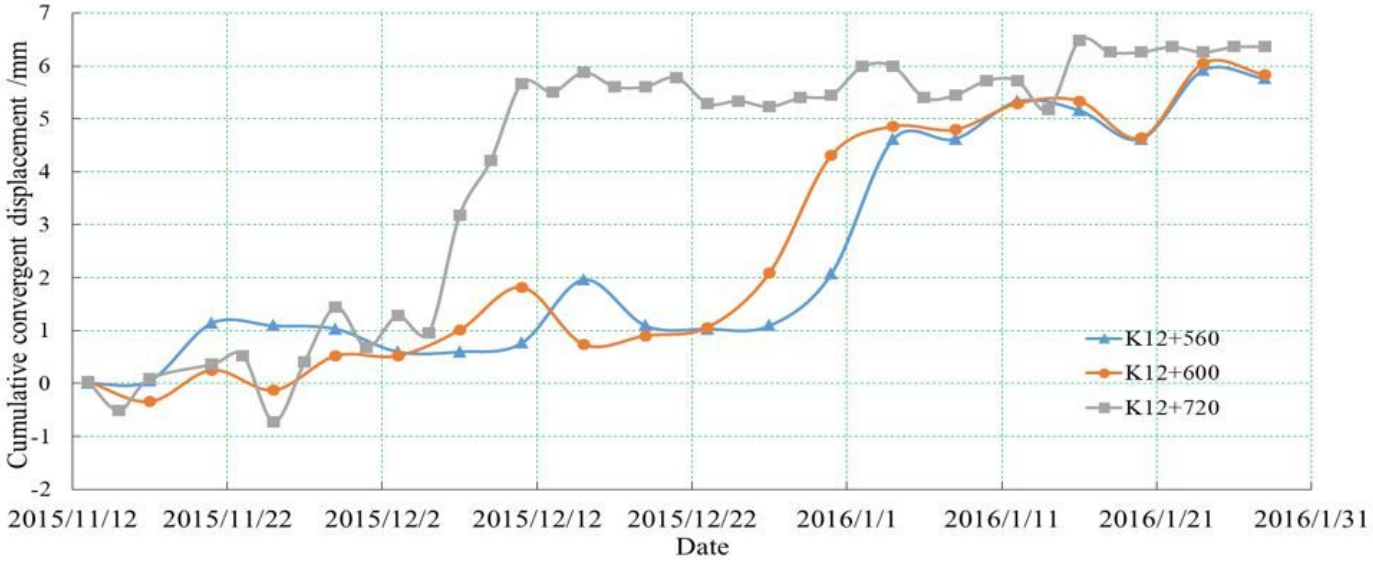

Figure 8

Displacement curves for tunnel within ancient landslide

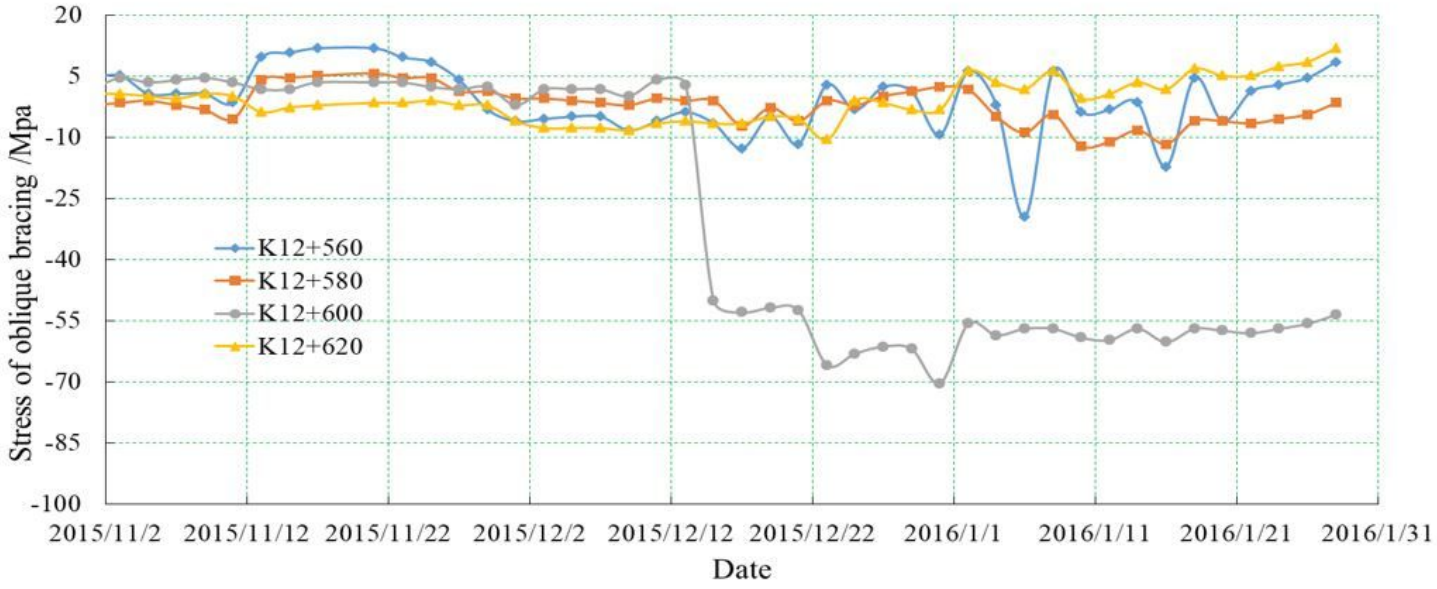

Figure 9

Stress curves for temporary oblique support

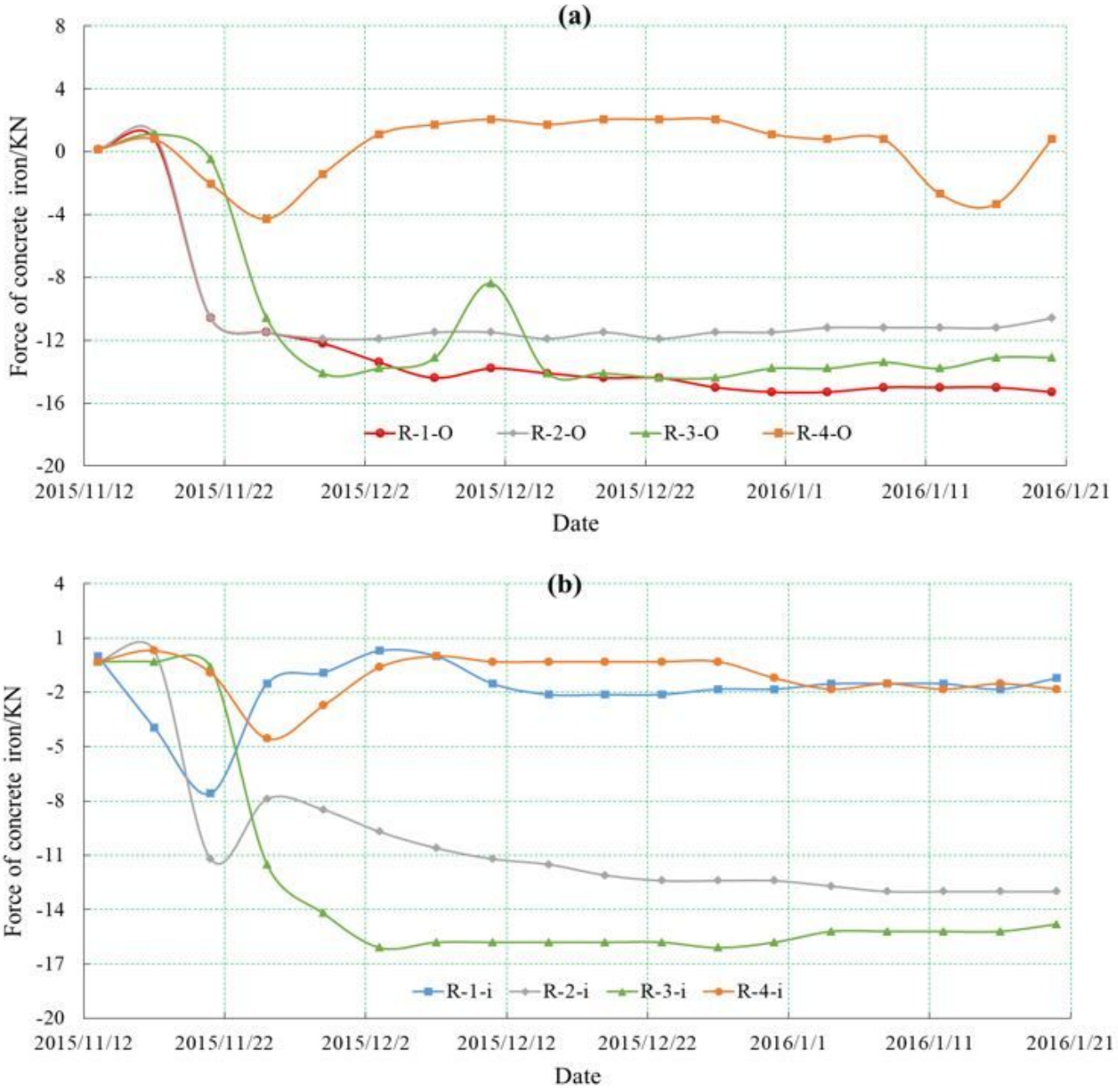

Figure 10

Stress curves of steel bar at K12+538. (a) in inner lining; (b) in outer lining.

Figure 11

Stress curves for concrete of secondary lining at K12+554

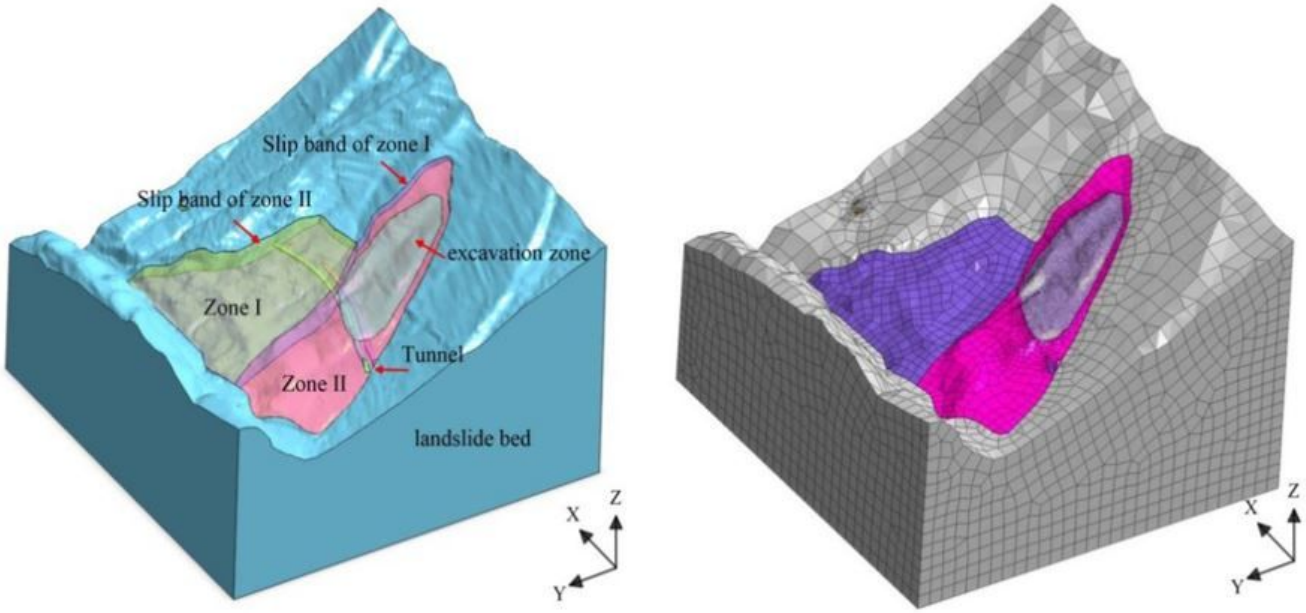

Figure 12

3D numerical model of landslide and tunnel

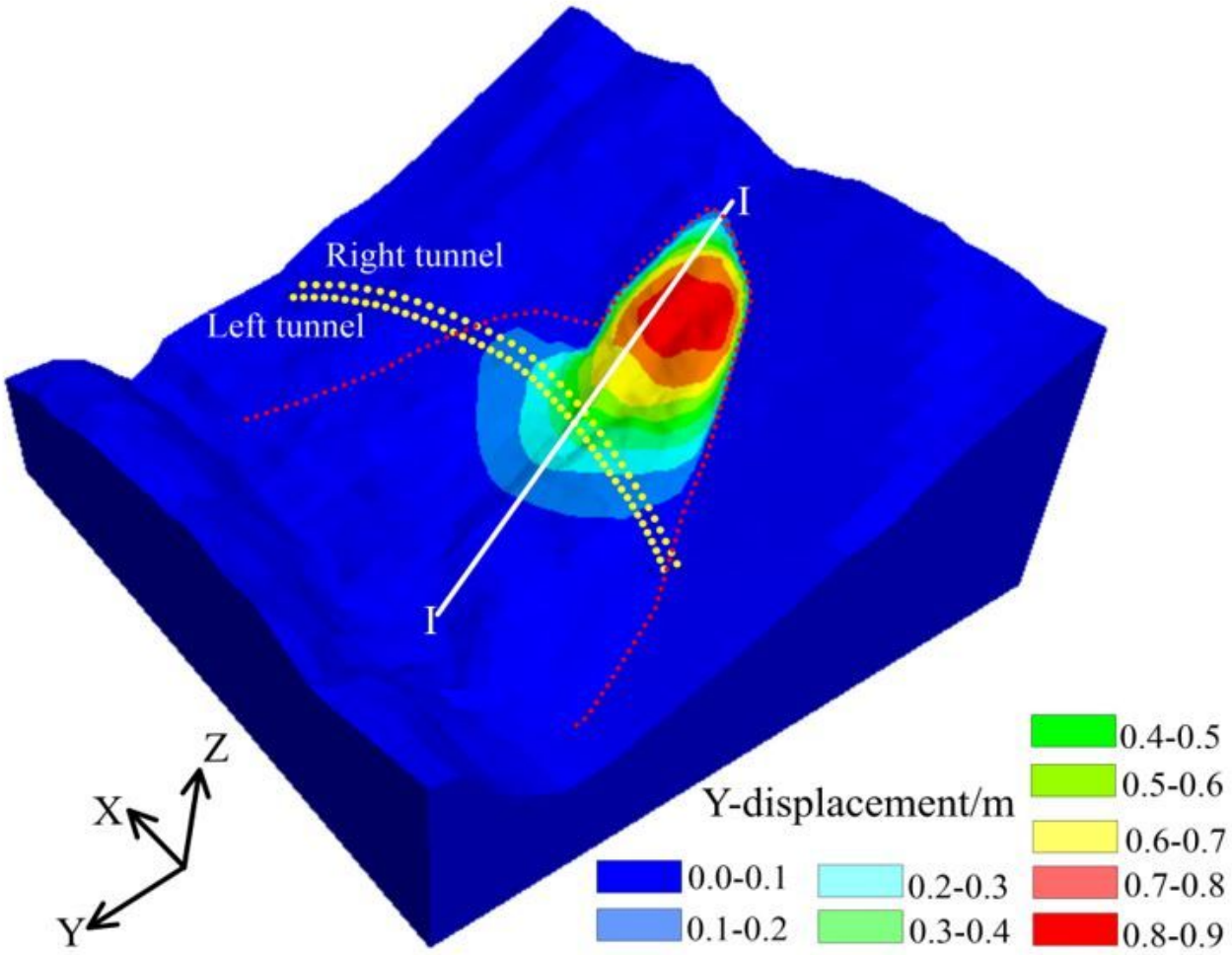

Figure 13

Y-displacement contour after completion of tunnel excavation (unit: m)

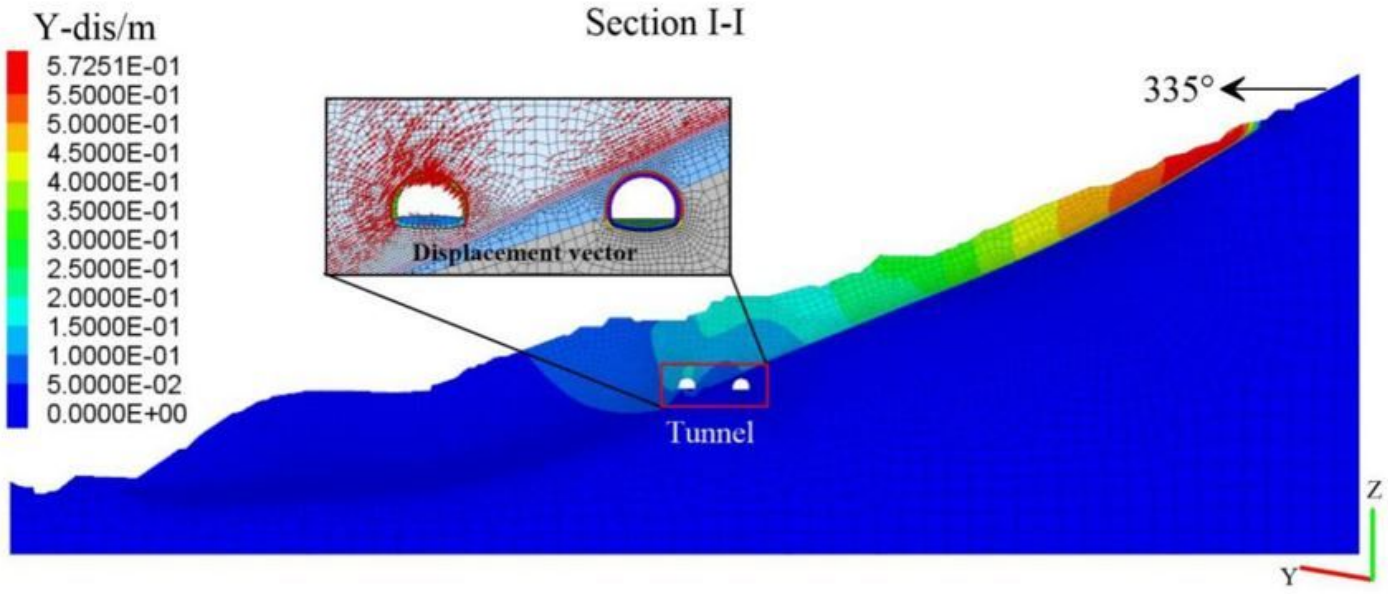

Figure 14

Y-displacement contour after tunnel excavation for typical section (I-I) (unit: m)

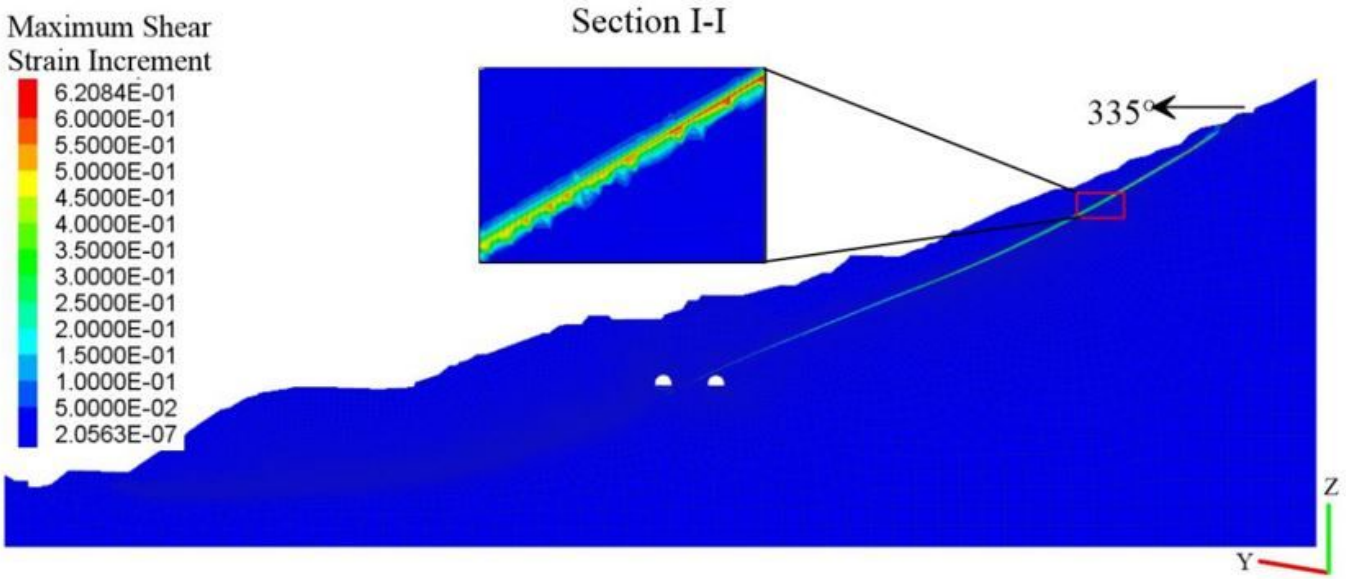

Figure 15

Maximum shear strain increment contour along section (I-I) after tunnel excavation

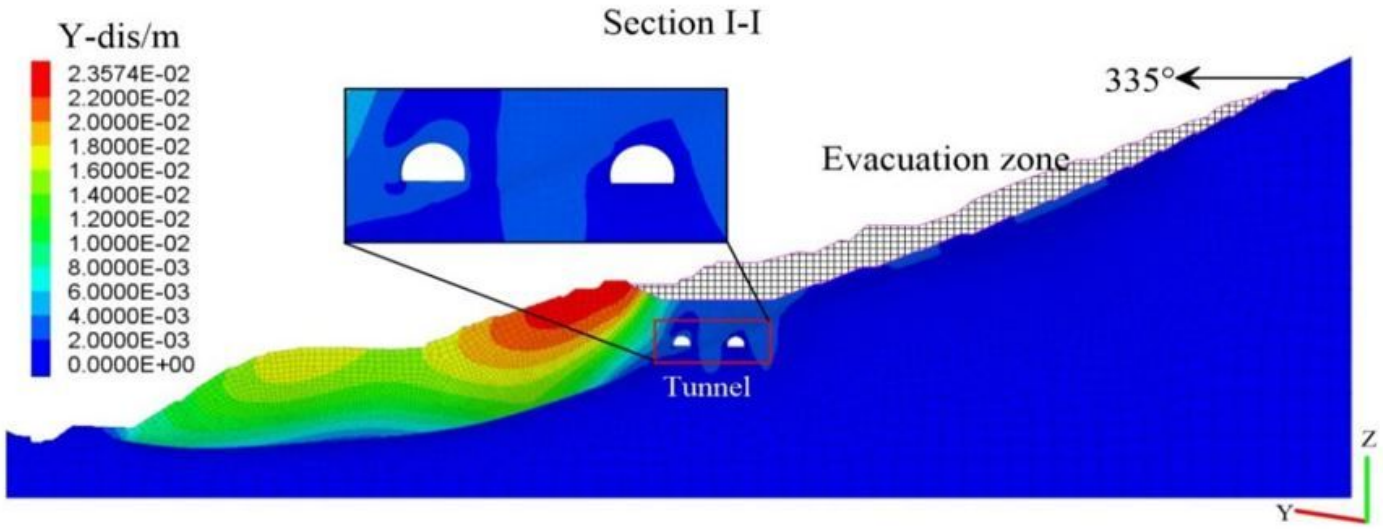

Figure 16

Y-displacement contour after soil removal along section I-I (unit: m)

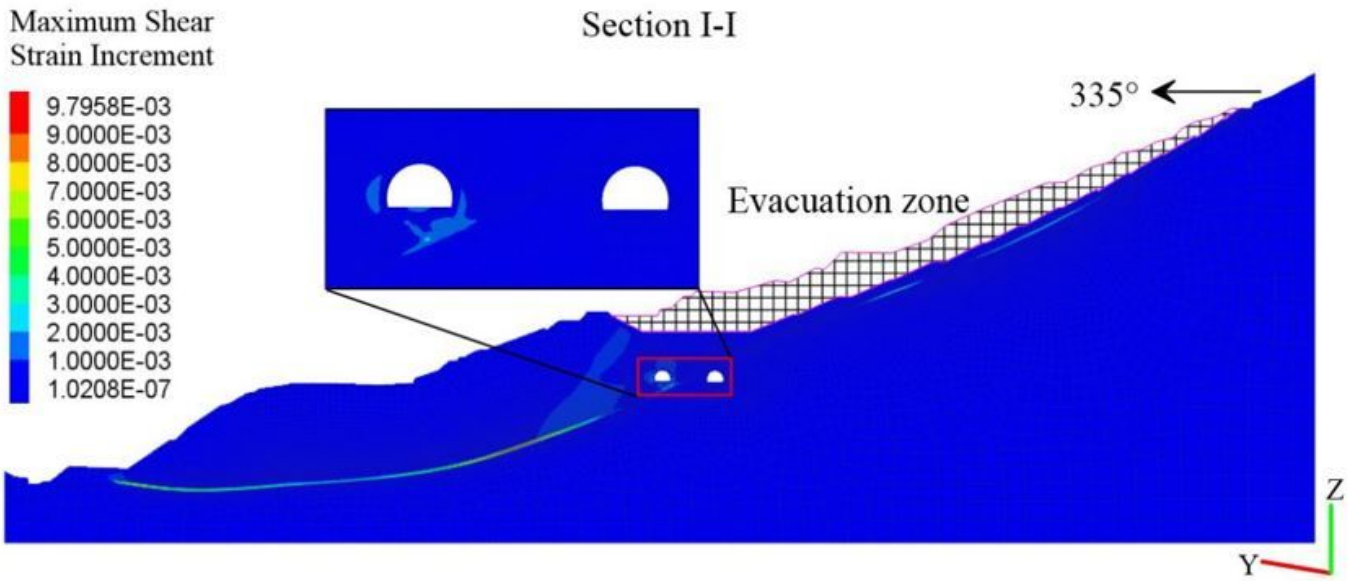

Figure 17

Maximum shear strain increment contour after soil removal along section I-I

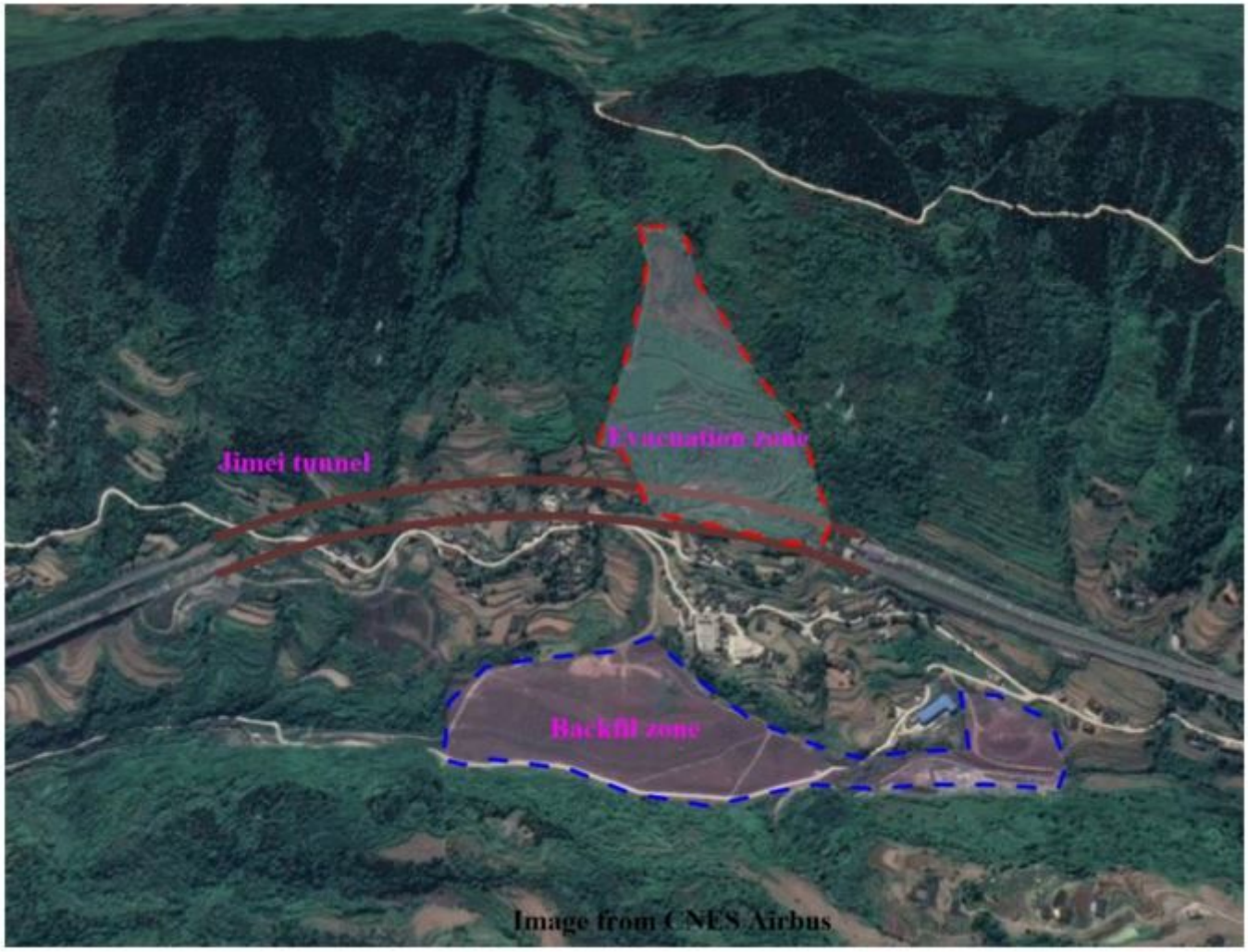

Figure 18

Bird view of construction site after soil removal Note: The designations employed and the presentation of the material on this map do not imply the expression of any opinion whatsoever on the part of Research Square concerning the legal status of any country, territory, city or area or of its authorities, or concerning the delimitation of its frontiers or boundaries. This map has been provided by the authors.